RAMAN SPECTROSCOPIC STUDIES OF LOAD TRANSFER IN MICROFIBRILLATED CELLULOSE/POLY(LACTIC ACID) COMPOSITES

A THESIS
SUBMITTED TO THE FACULTY OF THE GRADUATE SCHOOL
OF THE UNIVERSITY OF MINNESOTA
BY

Jin Yao

IN PARTIAL FULFILLMENT OF THE REQUIREMENTS
FOR THE DEGREE OF
MASTER OF SCIENCE

Dr. William Tai Yin Tze, Adviser

July, 2010

Acknowledgements

I am heartily thankful to my advisor, Dr. William Tai Yin Tze for his invaluable advice of this thesis. Dr. Tze has provided me with encouragement, guidance and support from the initial to the final level of my graduate program, without which I could not have finish this thesis. Also acknowledged are other members of my thesis committee, Dr. Shri Ramaswamy and Dr. Steven Severtson for their valuable suggestions on my thesis.

I owe my deepest gratitude to Dr. Jinping Dong for his assistance and training of Raman microscopy in Characterization Facilities and to Dr. Robert Seavey who has lent me the equipment for building my testing system. When I was building up my proposed testing system, Dr. Yong Chen, my college advisor, has given me numerous constructive suggestions. I also derived plentiful benefits from discussion with Mr. Weibin Guo. Without their support, my proposed research could not have been implemented.

I acknowledge the financial support from the National Research Initiative of the USDA Cooperative State Research, Education and Extension Service (grant number 2008-35504-19158) for funding my study. The composite samples were kindly supplied by Dr. John Simonsen and his graduate student Ms. Melissa Taylor (Oregon State University). Parts of this work were carried out in the Institute of Technology Characterization Facility, University of Minnesota, a member of the NSF-funded Materials Research Facilities Network (www.mrfn.org).

It has been good experience working with two of my colleagues, Ms. Lili Zhou and Mr. Jesse Lund, whose assistance are deeply appreciated.

Also deserving to be mentioned is my official affiliation at the University of Minnesota: the Department of Bioproducts and Biosystems Engineering. I thank Dr. Shri Ramaswamy, the head of the department, for opening up a wonderful learning experience by accepting me to the Master's program. I am grateful to Ms. Dorit Hafner and Ms. Susan Seltz, for taking care of my administrative-related business.

Last but not least, I would like to thank my parents, who always give me unfailing support and encouragement.

Dedication

This thesis/project is dedicated to my parents Wang Xiaoping and Yao Junma.

Abstract

The objective of this research was to investigate the feasibility of using Raman-tensile tests to evaluatethe transfer of load between polylactic acid (PLA) and cellulose nanofibers. Microfibrillated cellulose (MFC) was modified with oligomeric lactic acid. The modified MFC was loaded into a PLA solution before being cast into a film. The nanocomposite films were subjected to tensile loading during which Raman spectroscopy was performed under a microscope. The Raman spectrum of MFC was isolated from the spectrum of its composites. The stress-sensitive Raman band of cellulose (1095 cm^{-1}) was analyzed for wavenumber shift, which is an indication of load transfer from the PLA matrix to MFC. Compared to the control (untreated) sample, composites with lactide-treated MFC exhibited a higher Raman band shift as a response to both applied strain and stress, indicating an improved efficiency of load transfer across the compatibilized interphase between nanofibers and PLA. The effect of MFC addition ratio on the load transfer ability was also discussed. A higher MFC weight fraction (0.5 % versus 0.25 %) in the composite did not significantly affect the load transfer efficiency. This finding suggests that the efficiency of matrix/fiber load transfer at the local level is independent of the effects of macroscopic fiber-to-matrix ratio, at least at the (low) levels of MFC loading examined in this study. Overall, this research shows that it is feasible to use Raman spectroscopy to monitor load transfer in MFC/PLA composites for examining strategies aimed at improving adhesion and knowledge of the mechanism of PLA reinforcement by nano-cellulose.

Table of Contents

List of Tables

List of Figures

Chapter 1 Introduction

1.1. Background

Recently, there has been increasing research focus in producing composite materials with nano-sized reinforcement, i.e. nanocomposites. Nanocomposites can be defined as multiphase solid materials where one of the phases has one, two or three dimensions that is/are less than 100 nm, or structures having nano-scale repeated distances between the different phases that make up the material (Ajayan, Schadler, and Braun 2003). Because of this particular feature, nanocomposite exhibits extraordinary properties that are unachievable in conventional composites. In terms of mechanical properties, for example, nanocomposites have highly improved performance compared to traditional composites due to high aspect ratio of the reinforcing constituent and its remarkably high surface area to volume ratio. This implies that a relatively small amount of nanoscale reinforcement can have a noticeable effect on the macroscale properties of the composite. By adding only 1 wt% carbon nanotube in polystyrene, Qian *et al.* (2000) observed an increase in the elastic modulus and fracture stress of the resultant (composite) films by 36 – 42% and ~25% respectively.

In the meanwhile, due to growing environmental awareness, increased crude oil price and anxiety about global warming, there have been intensive attempts and interests to develop environmentally friendly and biodegradable products both in academic and industrial fields. Among these products, biocomposites based on raw materials derived from natural

resources are of great interests and have been a major subject in a large number of publications (Oksman *et al.* 2006)(Azizi Samir *et al.* 2005).

Polylactide (PLA) or poly(lactic acid), derived from sugar (e.g. of corn starch and sugarcanes), is a promising thermoplastic polyester because of its renewable resource-based origin along with its biodegradability and biocompatibility (Ragauskas *et al.* 2006). It can be degraded by simply hydrolyzing its ester bond without requiring the presence of hydrolysis catalytic enzymes (Garlotta 2001). PLA is an attractive sustainable alternative to petroleum-based plastics since it can be processed on standard plastic equipment. It can be molded, vacuum formed, blown or even extruded as easily as conventional plastics (Nakagaito *et al.* 2009). Among its many potential uses, PLA already has been applied in the medical field such as degradable implants and resorbable sutures (Grijpma *et al.* 2002), and also in packaging industry because of its resistance to fats and oils and ability to act as barriers to flavors and aromas (Tullo 2002).

Nonetheless, the inherent brittleness of PLA has been a major drawback for its large-scale commercial applications (Bhardwaj and Mohanty 2007).The impact strength of poly (L-lactide) approximates that of a relatively brittle polymer—polystyrene. In addition, the elongation at break of the PLA polymer is quite low, another indication of its brittleness (Anderson *et al.* 2008). Therefore, in order to improve the mechanical performance of PLA, toughening methods are needed.

Currently, numerous strategies have been employed to toughen polylactide materials, including altering stereochemistry, molecular weight and crystallinity of homopolymer,

synthesizing copolymers, and blending a second polymer or fiber (Anderson *et al.* 2008). Among these avenues of toughening polylactide, preparation of bionaoncomposites has become an attractive approach because of the renewability and biodegradability of both the material matrix and reinforcement agent (Oksman *et al.* 2006), and the high efficiency of nano-scale reinforcement for matrix materials.

One candidate of the reinforcing agents for PLA is cellulose, the main organic compound in plant species. Cellulose is composed of β-D-glucopyranose units bridged by (1→4)-glycosidic bonds. Cellulose molecules are linearly aggregated through van der Waals force and both intra- and intermolecular hydrogen bond (Gardner *et al.* 2008). Besides its abundance, renewability and biodegradability nature, cellulose has many advantages that entitle it as a promising candidate to reinforce composites, such as low energy consumption, low cost, low density, high specific strength and modulus, comparative ease of processablility, and availability of reactive surface for chemical fictionalization (Azizi Samir *et al.* 2005).

Linear cellulose chains in plant cell walls aggregate into microfibrils of 2 to 20nm in diameter, and several tens of microns in length (Azizi Samir *et al.* 2005). These microfibrils are embedded in a matrix of hemicelluloses and lignin to provide structural support to the cell wall. If these structural and nano-sized microfibrils can be isolated from plant cell walls and utilized as a reinforcing phase in composites, the performance of the resultant composites can be highly improved.

In 1980s, a new form of cellulose was first introduced by Turbak et al.(1983) and Herrick et al.(1983), called microfibrillated cellulose (MFC). This new form of cellulose is produced by imposing repeated high-pressure mechanical shearing forces on dilute slurries of cellulose fibers through a "homogenizing" machine (Herrick *et al.* 1983). This shearing action yields a highly entangled network which typically consists of elements (fibrils) having a wide distribution of diameter down to nanoscale (Herrick *et al.* 1983). Figure 1.1 is a scanning electron micrograph of MFC exhibiting a web-like structure of interconnected fibrils and microfibrils, the latter having diameters in the range from 10 to 100 nm. Two features of MFC are, (1) exceptionally large specific surface area, implying its potentially high capacity to interact with secondary components/materials (Stenstad *et al.* 2008), and (2) highly accessible by cellulase enzyme (Herrick *et al.* 1983), implying its biodegradability. These two outstanding features of MFC indicate that the surface chemistry of this stiff nano-cellulose can be potentially tuned to interact favorably with PLA to enhance mechanical properties of the bioplastic while maintaining its biodegradation advantage.

Apart from wood pulp fibers, sugar beet pulp (Dufresne *et al.* 1997), potato pulp (Dufresne *et al.* 2000) and skin of prickly pear fruits (Habibi *et al.* 2009) have been employed as raw materials to produce MFC. Since the introduction of MFC, several methods have been also developed to improve the preparation of MFC. Nakagaito and Yano (2004) carried out a refining procedure prior to the homogenizing treatment to gradually peel off the external cell wall layers (P and S1 layers), thereby exposing the S2 layer for the subsequent microfibrillation operation. Chakraborty *et al.* (2005) developed

a technique by which fibers after refining were cryocrushed under liquid nitrogen instead of going through homogenizer. The microfibrillation of cellulose by shearing actions alone typically suffers shortcomings such as high energy consumption due to the need for multiple passes through the homogenizer and process instability due to the frequent blockage at the homogenizer constrictions. In order to overcome such shortcomings, enzymatic hydrolysis pretreatment was introduced to prepare MFC with a well-controlled diameter along with high aspect ratio (Pääkkö *et al.* 2007).

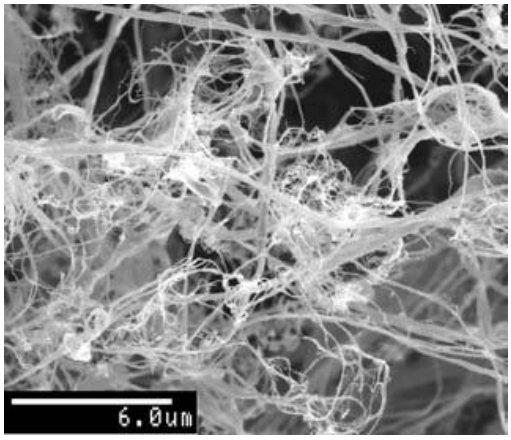

Figure 1.1 SEM micrograph of MFC from 30 passes through the refiner followed by 14 passes through the homogenizer pulp (Nakagaito and Yano 2004)

Because of its features like high aspect ratio and high surface to volume ratio, MFC have been employed as the reinforcement component in many composites. By impregnating MFC into phenolic resin, Nakagaito and Yano (2005) obtained a composite with a bending strength comparable to that of magnesium alloy, a widely used metal in electronic device castings due to its high specific strength. Bruce *et al.* (2005) embedded cellulose microfibrils into four different matrixes (polyvinylacetate, acrylic polymer, epoxy and hemicelluloses) and produced composites with mechanical properties within

the range of polyester composites filled with chopped strand mat glass fiber. Moreover, high toughness polysaccharide nanocomposites were produced by Svagan *et al.* (2007) using as high as 70 wt% MFC that was enzymatic pretreated to facilitate delamination of the fiber wall . Some research works have also been reported about using MFC to reinforce PLA due to the attractiveness of making sustainable biocomposites. By blending 10wt% MFC, Iwatake *et al.* (2008) obtained a PLA/MFC composite with 25% higher tensile strength and 40% higher Young's modulus than those of the neat PLA resin sheet, without reducing the yield strain. Chakraborty *et al.* (2005) also compounded PLA with cryocrushed MFC. Microfibrils were uniformly dispersed in the polymer matrix, but the mechanical properties of the composites were not reported in their paper. Nakagaito *et al.* (2009) developed a method similar to the papermaking procedures to produce MFC/PLA composites where a good dispersion of MFC was obtained even at high MFC contents. They studied the effect of MFC loading ratio on the mechanical properties of composites and found the modulus and strength of composites were improved as the content of MFC increased from 10 - 70 wt%.

In the current techniques of producing MFC, the cellulose microfibrils cannot be dispersed easily in non-polar media. Such restriction is detrimental if one wants to use these microfibrils to reinforce non-polar polymers, such as polyolefins (polyethylene and polypropylene) or other polymers that are less hydrophilic. Much research has been conducted to modify the surface of cellulose microfibrils in order to make them compatible with non-polar polymers and to increase the interfacial bonding (Stenstad *et al.* 2008; Lönnberg *et al.* 2008; Lönnberg *et al.* 2008; Gousséet *al.* 2004). One of surface

modification methods is to coat oligomer dispersant on MFC. Wang and Sain (2007b) studied the reinforcement effect of ethylene-acrylic oligomer emulsion coated MFC on polyethylene (PE) and polypropylene (PP). Compared to unfilled polymers(PP or PE)/acrylic blends, the composites with 5 wt% oligomer coated nanofibers exhibited significant improvement in modulus (62% and 92% for PE and PP, respectively) and tensile strength (26% and 146% for PE and PP, respectively). This favorable result verified the effective dispersion of MFC in hydrophobic matrixes. By grafting N-Octadecyl isocyanate on MFC, Siqueira *et al*. (2009) evaluated the effect of the grafting agent on the compatibility of MFC with polycaprolactone (PCL) matrix. They observed, compared to the neat PCL matrix, an increase (60%) in the modulus of the composites with only 3 wt% surface-modified MFC, but not in the case of unmodified MFC because of poor dispersibility of the latter. In another study, hydrophoblized MFC by three different coupling agents: 3-aminopropyltriethoxysilane, 3-glycidoxypropyltrimethoxysilane, and a titanate coupling agent (Lica 38), were employed to prepare composite films with epoxy as the matrix (Lu *et al.* 2008). A better dispersion and interfacial adhesion of MFC with epoxy were confirmed by dynamical mechanical analysis in the tension mode. For example, at a 3.7wt% addition of MFC treated with aminosilane, the storage modulus at 30 ℃ increased by about 25%, compared to neat epoxy. At 130 ℃ the modulus increase was more substantial – from about 10 MPa to over 65 MPa for composites filled with aminosilane-treated MFC.

1.2. Hypothesis and motivating questions

To evaluate the effectiveness of matrix polymer reinforcement, it is important to achieve an improved understanding of the factors that influence the mechanical properties of biocomposites. Such factors include properties of the reinforcing agent, the matrix polymer, and the interphase, as well as the distribution behavior of reinforcing medium in the matrix (Hoecker and Karger-Kocsis 1996). Among these factors, interfacial properties, specifically the transfer of load across the interphase between the matrix and reinforcing constituent, are not well understood (Tze *et al.* 2007).

Raman micro-spectroscopy, a technique that can be used to probe molecular deformations of polymers, has been proven a promising approach in the evaluation of load transfer in the cellulosic-fiber/polymer interphase (Tze *et al.* 2007). This method was established based on the effect of tensile stress on certain Raman bands of reinforcing units (cellulose), where a proportional shift in the wavenumbers is observed because of molecular chain stretching of the reinforcing unit during the deformation of composites (Young and Eichhorn 2007). Eichhorn *et al* (2001a) identified the stress-induced Raman bands of cellulose at 895 cm^{-1} and 1095cm^{-1}, which shift 0.4 cm^{-1} to lower wavenumbers for every 100 MPa increase in tensile stress.

Young and Eichhorn (2007) systematically reviewed literatures that report on the relationship between stress and Raman bands shift of synthetic and natural polymer fibers. They concluded that few studies were focused on the interfacial adhesion between a fiber and the matrix in composites, and no papers were published on monitoring the local deformation, thus interfacial behavior of two-phase bio-nanocomposites using

Raman spectroscopy. It can be inferred, therefore, from the review that interfacial properties of nanocomposites are under studied. Specifically, research that addresses interfacial properties of MFC/PLA nanocomposites would provide insights into approaches of toughening the polymer. This knowledge, once acquired, will ultimately improve the toughening efficiency in the manufacturing of mechanically enhanced PLA products.

Recent research indicates the promising applicability of Raman spectroscopy in the evaluation of load transfer for evaluating fiber/polymer adhesion (Tze *et al.* 2007). Although the nano-network MFC is quite different from rod-like fibers, this Raman technique is hypothesized to be applicable to MFC-reinforced polymers to allow the evaluation of the effectiveness of interfacial load transfer.

1.3. Thesis objectives and approach

The overall objective of this thesis was to investigate the feasibility of using Raman microscopy technique to evaluate the interfacial load transfer between microfibrillated cellulose (MFC) and poly(lactic acid) (PLA). To achieve this objective and test the aforementioned hypothesis, a two-step methodology has been adopted.

First, to identify stress-induced Raman band of MFC, a Raman spectra collection protocol was established by conducting Raman spectra collection experiments and also by referring to related publications. Second, nanocomposites of PLA blended with surface-modified or unmodified MFC at two loading levels were subjected to Raman spectroscopy while being stretched. The stress-sensitive Raman bands were analyzed for

wavenumber shift. The rate at which the MFC stresses increase, characterized by the amount of band shift, will indicate the efficiency of load transfer from the PLA matrix to the reinforcing phase (MFC).

In this study, a micro-tensile testing system was also set up considering the limited weight and space provided by the X-Y stage of the Raman microscopy systems employed in this research.

1.4. References

Ajayan PM, Schadler LS, Braun PV. (2003) Nanocomposite science and technology Weinheim : [Great Britain] : Wiley-VCH.

Anderson KS, Schreck KM, Hillmyer MA (2008) Toughening polylactide. Polymer Reviews 48(1):85.

Azizi Samir MAS, Alloin F, Dufresne A (2005) Review of recent research into cellulosic whiskers, their properties and their application in nanocomposite field. Biomacromolecules 6(2):612-626.

Bhardwaj R, Mohanty AK (2007) Modification of brittle polylactide by novel hyperbranched polymer-based nanostructures. Biomacromolecules 8(8):2476-2484.

Bruce DM, Hobson RN, Farrent JW, Hepworth DG (2005) High-performance composites from low-cost plant primary cell walls. Composites Part A: Applied Science and Manufacturing 36(11):1486-1493.

Chakraborty A, Sain M, Kortschot M (2005) Cellulose microfibrils: A novel method of preparation using high shear refining and cryocrushing. Holzforschung 59(1):102-107.

Dufresne A, Cavaillé J, Vignon MR (1997) Mechanical behavior of sheets prepared from sugar beet cellulose microfibrils. Journal of Applied Polymer Science 64(6):1185-1194.

Dufresne A, Dupeyre D, Vignon MR (2000) Cellulose microfibrils from potato tuber cells: Processing and characterization of starch-cellulose microfibril composites. Journal of Applied Polymer Science 76(14):2080-2092.

Eichhorn SJ, Sirichaisit J, Young RJ (2001) Deformation mechanisms in cellulose fibres, paper and wood. Journal of Materials Science 36(13):3129-3135.

Gardner DJ, Oporto GS, Mills R, Azizi Samir M,Ahmed Said (2008) Adhesion and surface issues in cellulose and nanocellulose. Journal of Adhesion Science and Technology 22:545-567.

Garlotta D (2001) A literature review of poly(lactic acid). Journal of Polymers and the Environment 9(2):63-84.

Gousséé C, Chanzy H, Cerrada ML, Fleury E (2004) Surface silylation of cellulose microfibrils: Preparation and rheological properties. Polymer 45(5):1569-1575.

Grijpma DW, Altpeter H, Bevis MJ, Feijen J (2002) Improvement of the mechanical properties of poly(D,L-lactide) by orientation. Polymer International 51(10):845-851.

Habibi Y, Mahrouz M, Vignon MR (2009) Microfibrillated cellulose from the peel of prickly pear fruits. Food Chemistry 115(2):423-429.

Herrick FW, Casebier RL, Hamilton JK, Sandberg KR (1983) Microfibrillated cellulose: Morphology and accessibility. Journal of Applied Polymer Science: Applied Polymer Symposium 37(815):827.

Hoecker F, Karger-Kocsis J (1996) Surface energetics of carbon fibers and its effects on the mechanical performance of CF/EP composites. Journal of Applied Polymer Science 59(1):139-153.

Iwatake A, Nogi M, Yano H (2008) Cellulose nanofiber-reinforced polylactic acid. Composites Science and Technology 68(9):2103-2106.

Lönnberg H, Fogelström L, Berglund L, Malmström E, Hult A (2008) Surface grafting of microfibrillated cellulose with poly(ε-caprolactone) – synthesis and characterization. European Polymer Journal 44(9):2991-2997.

Lu J, Askeland P, Drzal LT (2008) Surface modification of microfibrillated cellulose for epoxy composite applications. Polymer 49(5):1285-1296.

Nakagaito AN, Yano H (2005) Novel high-strength biocomposites based on microfibrillated cellulose having nano-order-unit web-like network structure. Applied Physics A: Materials Science & Processing 80(1):155-159.

———. (2004) The effect of morphological changes from pulp fiber towards nano-scale fibrillated cellulose on the mechanical properties of high-strength plant fiber based composites. Applied Physics A: Materials Science & Processing 78(4):547-552.

Nakagaito AN, Fujimura A, Sakai T, Hama Y, Yano H (2009) Production of microfibrillated cellulose (MFC)-reinforced polylactic acid (PLA) nanocomposites from sheets obtained by a papermaking-like process. Composites Science and Technology 69(7-8):1293-1297.

Oksman K, Mathew AP, Bondeson D, Kvien I (2006) Manufacturing process of cellulose whiskers/polylactic acid nanocomposites. Composites Science and Technology 66(15):2776-2784.

Pääkkö M, Ankerfors M, Kosonen H, Nykänen A, Ahola S, Österberg M, Ruokolainen J, et al. (2007) Enzymatic hydrolysis combined with mechanical shearing and high-pressure homogenization for nanoscale cellulose fibrils and strong gels. Biomacromolecules 8(6):1934-1941.

Qian D, Dickey EC, Andrews R, Rantell T (2000) Load transfer and deformation mechanisms in carbon nanotube-polystyrene composites. Applied Physics Letters 76(20):2868-2870.

Ragauskas AJ, Williams CK, Davison BH, Britovsek G, Cairney J, Eckert CA, Frederick WJ, Jr., et al. (2006) The path forward for biofuels and biomaterials. Science 311(5760):484-489.

Siqueira G, Bras J, Dufresne A (2009) Cellulose whiskers versus microfibrils: Influence of the nature of the nanoparticle and its surface functionalization on the thermal and mechanical properties of nanocomposites. Biomacromolecules 10(2):425-432.

Stenstad P, Andresen M, Tanem B, Stenius P (2008) Chemical surface modifications of microfibrillated cellulose. Cellulose 15(1):35-45.

Svagan AJ, Azizi Samir, My A. S., Berglund LA (2007) Biomimetic polysaccharide nanocomposites of high cellulose content and high toughness. Biomacromolecules 8(8):2556-2563.

Tullo AH (2002) Breaking the bank with new polymers. Chemical Engineering News 80:13.

Turbak AF, Snyder FW, Sandberg KR (1983) Microfibrillated cellulose, a new cellulose product: Properties, uses, and commercial potential. Journal of Applied Polymer Science: Applied Polymer Symposium 37:815-827.

Tze W, O'Neill S, Tripp C, Gardner D, Shaler S (2007) Evaluation of load transfer in the cellulosic-Fiber/Polymer interphase using a micro-raman tensile test. Wood and Fiber Science 39(1):184-195.

Wang B, Sain M (2007) Isolation of nanofibers from soybean source and their reinforcing capability on synthetic polymers. Composites Science and Technology 67(11-12):2521-2527.

Young RJ, Eichhorn SJ (2007) Deformation mechanisms in polymer fibres and nanocomposites. Polymer 48(1):2-18.

Chapter 2 Literature review

2.1. Introduction

Composites exhibit properties that cannot be achieved with either of the constituents alone. One of the purposes of producing composites is to improve the mechanical properties of one constituent by using the other constituent as a reinforcing agent, while retaining other properties of the constituent. For example, fibers are strong and stiff. Plastics are considerably resistant to chemicals. By combing fibers and plastics, it is possible to produce a material with the strength and stiffness close to that of fibers and the chemical resistance of the plastics (Tripathi and Jones 1998).

In composites, a boundary region, called interphase, is inevitably created between matrix and reinforcing phase. An interphase can be defined as "the region of significantly changed chemical composition that constitutes the bond between the matrix and reinforcement" (Kim 1998). The properties of an interphase are primarily determined by the chemical/morphological nature and physical/thermodynamic compatibility between the two constituent components, and these interfacial properties influence the overall performance of the composites. Therefore, to obtain a thorough knowledge of interfacial region becomes an indispensable avenue to the successful design and proper use of composite materials (Tripathi and Jones 1998).

Among many properties of interphase in composites, the transfer of load (or stress) between reinforcement and matrix has drawn much attention due to its role in improving the mechanical properties of the matrix polymer. An interphase with highly efficient load transfer ability allows a large portion of applied load to be transferred to high-

performance fibers, thereby improving the strength and modulus of the constituted composite. Therefore, measuring and evaluation of the load transfer ability across the interphase are critical tasks in the engineering of composite materials to control mechanical performance.

In this chapter, a comprehensive literature review is described about different techniques for the measurement of the load or stress transfer in composites containing different reinforcing agents down to nano-scale. These techniques are evaluated based on their feasibility of application to composites with different reinforcing agents, especially nano-fibers.

2.2. Stress or load transfer measurement in composites with micro-fibers

Fiber fragmentation tests are widely employed to measure the ability of the interphase to transfer load (or stress) between fibers and matrix because of its simplicity in specimen preparation, ease of testing and wealth of information obtained from the fracture processes (Tripathi and Jones 1998). The principle of this technique is to stretch a composite specimen embedded with a single fiber to a saturation state where the fiber is no longer able to fracture into shorter lengths (Figure 2.1). The shortest fragment length is called the critical fiber length (l_c) (Tripathi and Jones 1998). This parameter is correlated with the average interfacial shear strength, a value that quantifies the efficiency of fibers in carrying load at the interphase, based on a shear model first proposed by Kelly and Tyson (1965). Several more sophisticated models have been developed later to take into account of the actually complex situation during fiber fragmentation tests (Tripathi and Jones 1998) (Kim *et al.* 1993). The fiber fragment length can be measured by optical

microscope for transparent matrix composites. Another technique called acoustic emission technique was also employed to monitor the number of fiber fragments during the test, particular for non-transparent matrix materials (Roman and Aharonov 1992).

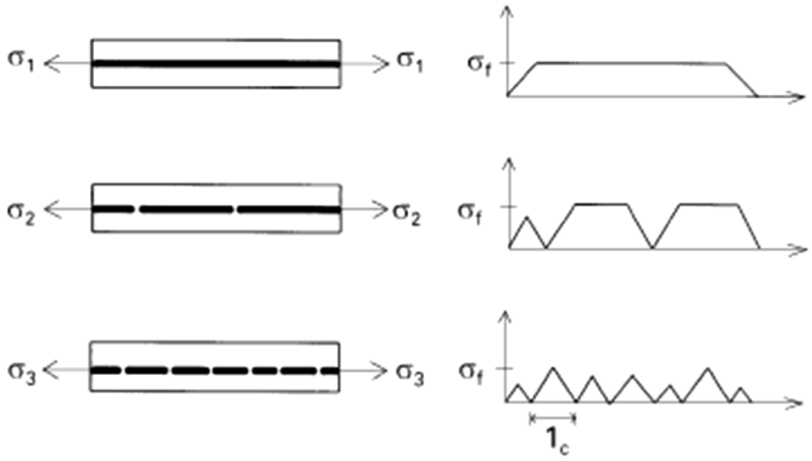

Figure 2.1 A schematic drawing of the fragmentation test (Tripathi and Jones 1998)

One of the main applications of fiber fragmentation test is to assess the effect of different surface treatments on the stress or load transfer capacity of the interphase. For example, the interfacial shear strength of composites made of glass fibers treated with different coupling agents in epoxy and vinyl ester resin was studied by using fiber fragmentation tests (Cheng *et al.* 1993). In addition, Schultz *et al.* (1987) utilized fiber fragmentation tests to evaluate the effect of oxidization treatments on the ability of the interphase to transfer stress from the epoxy to the carbon fibers. Drazal and Madhukar (1993) also studied the effect of carbon fibers surface treatments on the interfacial adhesion using fiber fragmentation tests and correlated the results with the data obtained from macromechanical (bulk) tests. They concluded that the composite properties could only be explained when both the fiber-matrix adhesion and fracrure are considered.

Conventional fiber fragmentation tests are limited by the lack of an accurate data reduction technique. Two critical requirements for an accurate data reduction technique are: (1) an accurate stress transfer model that considers materials properties and different fracture behaviors during the test and (2) a characteristic parameter for the interphase that are based on the interfacial shear strength, fracture energy for crack growth along the interface region, or the efficiency of stress transfer between matrix and fiber (Tripathi and Jones 1998). On the other hand, the correlation of results obtained from micromechanical tests, in particular the fragmentation test, to the macromechanical properties of composite materials is still uncertain, and a direct relationship between the two dimensional scales of tests is still absent (Tripathi and Jones 1998).

Another micromechanical technique to measure the stress or load transfer capacity of an interphase is the fiber pull-out test (Figure 2.2a). In this test, a fiber partially embedded in a matrix block is loaded under tension at the free end while the matrix is fixed. As the load applied on the fiber increases, the fiber is pulled out of the matrix, while the load and displacement are recorded during the whole debonding process. The interfacial shear bond strength can be determined from the test. Although fiber pull-out tests can be used for many reinforcing fibers and different matrix polymers, there are some limitations associated with the maximum embedding length of the fiber above which the required pull-out force would be so strong that the fibers are broken before debonding occurs (Kim 1998). This limitation causes experimental difficulties and large data scatter for composites with strong interfacial bonding and small fiber diameters.

To overcome the difficulties encountered in the conventional fiber pull-out test, a modified testing technique called microdebond test (Figure 2.2b) has been developed (Miller *et al.* 1991). In this technique, a microdroplet resin is cured on the fiber so that the stress concentration at the fiber entry can be reduced to certain extent because of the smooth curvature at the boundary between the fiber and the microdroplet (Kim 1998). Although this technique can be employed for any combination of fiber and polymer matrices, it has several serious limitations resulting from the nature of the specimen and loading condition (Herrera-Franco and Drzal 1992). The state of stress in the microdroplet varies with the size and location of points of contact between the shearing blades (or microvise; Figure 2.2b) and the microdrop. Additionally, the presence of a meniscus around the fiber has a large effect on the interfacial stress, thus making the practice of calculating an average shear strength value questionable.

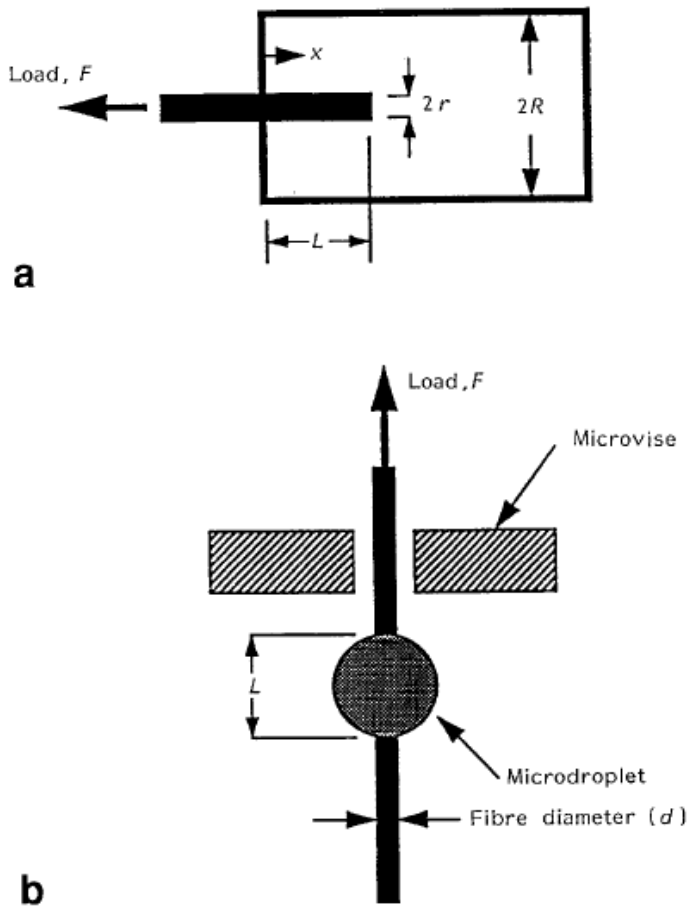

Figure 2.2 Schematic representation of the (a) fiber pull-out and (b) microbond techniques (Herrera-Franco and Drzal 1992)

Another tool, synchrotron microfocus X-ray diffraction (Figure 2.3), was employed to study the stress transfer mechanism in two-phase polymer systems (Young *et al.* 2004). This technique is based on the observation that when subjecting fibers to tension, the position of the reflections from meridional diffraction would shift due to the change of crystal strain, the amount of which corresponds to the stress on the fibers (Davies *et al.* 2001). For the composite specimen, a subtraction procedure was performed to isolate the diffraction patterns of fibers in the composites. Then the stress distribution on the fibers can be determined from the calibration data obtained from diffraction patterns of

individual stressed fibers. The interfacial shear stress was then calculated from the fiber stress distribution based on the shear-lag analysis (Shyng *et al.* 2006). This technique was applied to study matrix-to-fiber load transfer in composites made of epoxy resin and highly crystalline micro-scale fibers: poly(*p*-phenylene benzobisoxazole) (with diameters about 11 μm) or poly(*p*-phenylene terephthalamide) (with diameters about 12 μm) (Shyng *et al.* 2006). To study the interfacial stress transfer from fibers to matrix, microdroplet specimens were prepared with fibers and resin similar to the above (Eichhorn *et al.* 2006). The stress of fibers in the microdroplet specimen was mapped along the fiber both inside and outside the embedded area, as a function of applied stress. Then the interfacial shear stress values were calculated using a modified pull-out shear lag model with an interfacial failure criterion (Eichhorn *et al.* 2006).

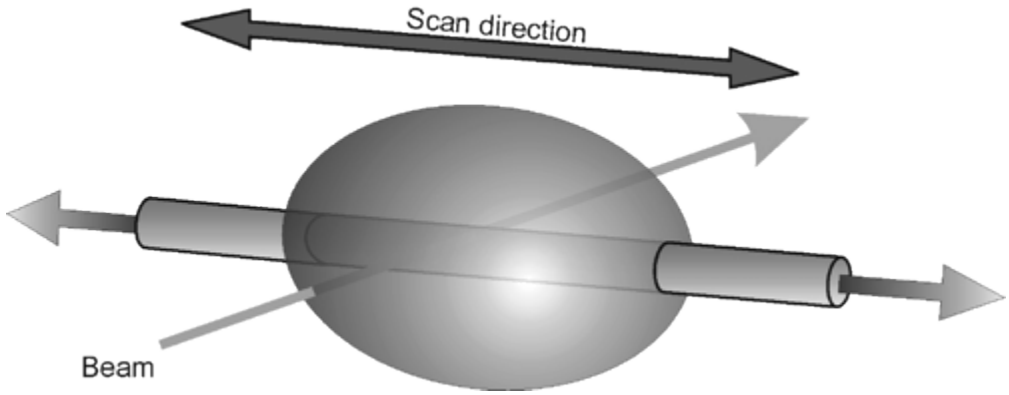

Figure 2.3 Schematic diagram of the experimental setup for synchrotron microfocus X-ray diffraction study (Young *et al.* 2004)

One advantage of the synchrotron X-ray diffraction technique is the capability to obtain X-ray diffraction pattern from an opaque matrix. This advantage implies that the technique can be extended to investigating the interfacial stress transfer between fibers and an opaque matrix, such as polypropylene (Shyng *et al.* 2007). However, this

technique may not be used to study the stress transfer mechanism in composite systems reinforced with low crystallinity fibers because of difficulty in acquiring well-defined X-ray diffraction patterns. In addition, X-ray induced radiation damage potentially limits the application of this technique.

2.3. Stress or load transfer measurement in nanocomposites

Nano fibers have substantially large surface area and, if rod-shaped, also a high aspect ratio, thus they have a high potential to improve the mechanical performance of composites compared to micron-scale fibers. However, the nano size does not guarantee an outstanding performance of nanocomposites. The effective application of nano fibers in composites is also strongly dependent on the nature and strength of the interphase between the reinforcement and matrix components as well as the fiber dispersion in the matrix (Ganesan and Lou 2009). Therefore, the measurement of stress or load transfer at the interphase becomes particularly important in the development of high performance nanocomposites.

However, due to the technical difficulties involved in handling objects at nanoscale, the measurement of the extent and efficiency of stress or load transfer through the interphase has been a great challenge in the study of polymer nanocomposites (Wagner and Vaia 2004). Only few experimental methods were reported about the direct measurement of the stress or load transfer capacity of the interphase, and the techniques have not been fully developed (Wagner and Vaia 2004).

Currently, studies of the transfer of stress or load between nano fibers and matrix materials rely on indirect measurements. These approaches involve complementing classical bulk mechanical tests with microscopic qualitative analysis. Liu *et al.* (2007) performed tensile tests on carbon nanotube/polyetherimide films. Their testing results showed that at an addition of 1 wt% carbon nanotubes, the elastic moduli of the nanocomposites were significantly improved by about 250%. They postulated that the improvement was due to the strong interfacial interaction that favors stress or load transfer between the nanotubes and matrix material. This postulation was derived from observing the fracture surfaces under a scanning electron microscope (SEM), which depicted the presence of many broken but embedded carbon nanotubes in the matrix and absence of debonding of nanotubes from the matrix. Qian *et al.* (2000) prepared carbon nanotube/polystyrene composites and observed improved elastic modulus (36 – 42%) and increased failing stress (~25%) at only 1 wt% nanotube addition. The stress or load transfer mechanism was studied by *in situ* transmission electron microscopy (TEM). A similar microscopic technique was also employed by Hwang *et al.* (2004) to provide supportive information about the efficiency of stress or load transfer between carbon nanotubes grafted with poly(methyl methacrylate) (PMMA) and commercial PMMA matrix. Under TEM, the tensile load was induced by charge accumulation, resulting in cracks bridged by carbon nanotubes. During the propagation of the crack, the carbon nanotube was gradually pulled out from the matrix, a qualitative analysis of the load transfer between the nanotube and the matrix was consequently obtained.

The concept of the aforementioned technique resembles that of conventional fiber pull-out tests. Indeed, several studies were reported on using pull-out tests to assess the interfacial strength, thus the capacity of stress or load transfer at the nanoscale. Cooper *et al.* (2002) developed a technique where carbon nanotubes bridging across voids in an epoxy matrix was drawn out using the tip of a scanning probe microscope while the forces involved were recorded (Figure 2.4). The force-displacement data were then correlated with the transmission electron micrographs of the specimen prior and subsequent to the tip action. Based on the experiments, the nanotube-polymer interfacial shear strength was estimated. The results supported the prediction that the interfacial strength of nanotube-polymer composites can be significantly higher than that of fiber-polymer composites measured using a similar technique (Cooper *et al.* 2002). Later, this technique was adapted by Barber *et al.* (2003) to measure the interfacial strength between a single multiwalled carbon nanotube and a polymer matrix. In their experiment, a carbon nanotube was directly attached to the tip of an atomic force microscopy (AFM) and pushed into a melt of polyethylene-butene. The polymer was then solidified around the carbon nanotube with the AFM tip attached. The single nanotube was then pulled out from the polymer with the forces acting on the nanotube recorded from the deflection of the AFM cantilever (tip). From the measured pull-out forces and embedded lengths, the interfacial fracture energy between single muliwalled carbon nanotubes and the polyethylene-butene matrix was estimated. The estimated value is comparable to that of fiber pull-out in other engineering composite systems such as glass fiber embedded in

maleic anhydride modified polypropylene, vinyl ester, polyamide 6 and polyamide 6,6 (Barber *et al.* 2004).

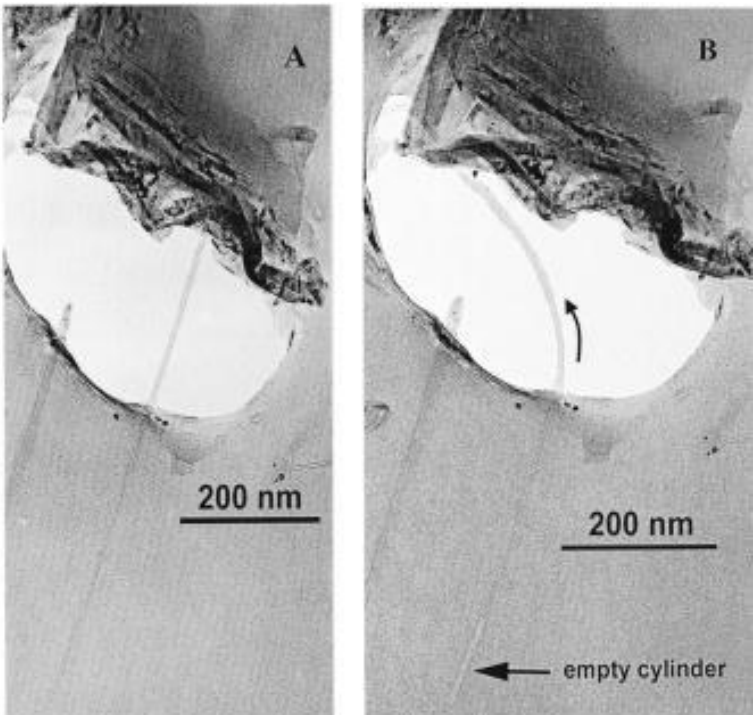

Figure 2.4 TEM images of a carbon nanotube crossing a void in an epoxy resin matrix. (a) TEM image of nanotube bridging matrix void. The bridging nanotube in these images has a diameter of 8.2 nm. (b) TEM image of same specimen following partial pullout by means of a SPM tip. The larger arrow shows the direction of the tip movement; the small arrow indicates the empty cylindrical hole left behind after partial pullout. (Cooper *et al*. 2002)

The nano pull-out technique was also applied to study the effect of carbon nanotube surface-chemical modification on the efficiency of stress (load) transfer in polymer composites filled with the nanotubes (Barber *et al.* 2006). Results showed that increased forces were required to pull each nanotube out of the polymer as the embedded length increased. Additionally, chemically modified nanotubes exhibited larger pullout forces compared to the pristine unmodified ones. The maximum interfacial shear strength derived from shear-lag calculations showed that a considerable increase in the interfacial

shear strength is obtainable by chemical modification of the nanotube surface to promote chemical bonding to the matrix material. Due to the improved adhesion between modified fibers and matrix polymer, the maximum embedding length had to be reduced to allow measurement of pullout forces prior to the occurrence of fiber fracture.

Nano-sized reinforcing elements were also observed to break into smaller fragments in the matrix polymer when the composites were subjected to load. This fragmentation phenomenon can also be employed to estimate the stress (load) transfer ability of the interphase formed between nano-fibers and polymer matrix. Wagner *et al.* (1998) studied single nanotube fragmentation by applying a tensile load on thin polymeric films containing multiwalled carbon nanotubes. The fragment length was measured under TEM. Based on a formula generalized from the classical model of Kelly and Tyson, the stress (or load) transfer efficiency in the nanocomposite was estimated, and the value was at least one order of magnitude higher than that in conventional fiber-based composites.

Another approach for measuring interfacial stress or load transfer ability in nanocomposites is based on spectroscopy. Near-infrared band gap photoluminescence was employed to study the stress (or load) transfer ability of the interphase between poly(methylmethacrylate) and semiconducting singlewalled carbon nanotubes (Leeuw *et al.* 2008). In this method, the fluorescence spectra of individual nanotubes embedded in polymer films were measured during the application of tensile and compressive strains. The band gaps of nanotubes were found to proportionally shift with strain at low strain levels. At high strain levels, the shift deviated markedly from linearity due to the loss of nanotube-host adhesion, suggesting slippage of individual nanotubes within the matrix.

The concept of correlating spectral shift with applied stress or strain can be traced to 1977 when the frequency or wavenumber of the Raman bands of polydiacetylene crystal fibers was reported to shift as a response to the stress (load) applied to the fibers (Mitra *et al.* 1977). Since then, a large number of experiments have been conducted based on this concept. The following sections will focus on the application of this concept, specifically using Raman spectroscopy, to the study of stress (or load) transfer at the composite interphase.

2.4. Stress or load transfer measurement using Raman spectroscopy

Raman spectroscopy is based on the Raman scattering phenomenon where a very small amount of light is inelastically scattered at a different frequency from that of the incident light. This part of the scattered light carries information about molecular vibration in materials, and therefore it can be used to characterize molecule deformation of polymer materials.

In 1977, Mitra *et al.* (1977) reported that when a monocrystalline fiber of polydiacetylene was subjected to a tensile loading, two of its Raman peaks linearly shifted to lower wavenumbers with elongation. They concluded that the principal contribution to this observation is due to the bond anharmonicity, rather than to stress-induced changes in electron delocalization. Based on this assumption, models were developed to calculate peak shift of the two Raman bands as a response to fractional elongation (strain). The prediction from models closely agreed with the experimental data.

The stress- or strain-dependent band shift behavior was later confirmed by many other researchers on different types of high-performance fibers. Day *et al.* (1987) strained high modulus poly(p-phenylene benzobisthiazole) fibers, collected Raman spectra using a 10 mW He-Ne laser, and observed that three peaks at 1175, 1480 and 1600 cm^{-1} shifted to lower frequencies as a response to the applied strain. Among them, the 1480 cm^{-1} peak exhibited the highest sensitivity to strain, with a shift rate in the order of -12.1 cm^{-1}/% strain. Young *et al.* (1990) also reported a similar behavior in poly(p-phenylene benzobisoxazole) fibers. They identified three strain-sensitive Raman peaks with the 1280 cm^{-1} being the most sensitive, shifting by -7.9 cm^{-1}/% strain.

One type of high-performance fibers that has been widely used in many areas is carbon fibers, which also exhibit a shift of specific Raman peaks with the application of tensile loading. Robinson *et al.* (1987) studied the strain dependence of the Raman frequencies for polyacrylonitrile (PAN)-based, rayon-based, and pitch-based carbon fibers. They analyzed the Raman spectra in the region of 1200 to 1800 cm^{-1} for the three types of carbon fibers and observed two peaks at 1580 and 1360 cm^{-1} that shifted to lower frequencies under the application of a tensile strain or stress. The band at about 1580 cm^{-1} corresponds to the C-C in-plane stretching mode of the graphite planes of an infinite crystal, while the other band (1360 cm^{-1}) was attributed to the crystal boundaries of the graphite.

Bio-based fibers have also been observed to exhibit Raman band shifts under external deformation. For regenerated cellulose fibers, Hamad and Eichhorn(1997) identified two peak positions at 895 and 1095 cm^{-1}, that shifted to lower wavenumbers due to the tensile

stress or strain on the cellulose chains. They also reported that the shift of both peak positions was more significant related to molecular stress than strain. Later, Eichhorn *et al.* (2001b) observed that the strain sensitivity of the Raman band shift (in cm^{-1}/%) increased with the Young's modulus of regenerated cellulose fibers, while the stress-dependent band shift was universally about -4cm^{-1}/GPa for both Raman peaks at 895 and 1095 cm^{-1}.

On natural cellulose fibers, Eichhorn *et al.* (2001a) observed that the 895 cm^{-1} peak found in regenerated cellulose fibers was absent in the Raman spectra of steam exploded flax and field retted hemp fibers. They further observed that the peak at 1095 cm^{-1}, corresponding to the stretching of the cellulose ring structure, shifted towards a lower wavenumber during tensile deformation. They also demonstrated that the rate of Raman peak shift was invariant with stress for all cellulose fiber types examined in the report, which was in consistent with their proposed fiber microstructure model.

Gierlinger *et al.* (2006) stretched single wood fibers to study molecular changes by using Raman microscopy. Strong correlations were found between the shift of the band at 1097cm^{-1} and the applied stress and strain. They also observed a decrease in the band height ratio of the 1127 cm^{-1} and 1097cm^{-1} as the fibers were strained, which was explained as a consequence of the torsion angle widening of the glycosidic C-O-C bond.

The strain- or stress-sensitive bands of a fiber material can be used to study load transfer in a composite filled with the same fiber. Paipetis and Galiotis (1996) applied this technique to carbon-fiber/epoxy model composites. They first established the relationship

between the band shift of the E_{2g} in-plane vibration of the graphitic cell as a function of applied stress. They then collected Raman spectra at different locations along the carbon fiber embedded in epoxy, and converted, using the calibration curve, the band shift at each location to produce a stress distribution profile. By using this stress profile along the fiber/polymer interphase, the interfacial shear stress was calculated using an equation derived from the balance of forces. Using this method, it was found that fiber sizing treatments improved the efficiency of matrix-to-fiber stress transfer, and the effect was attributed to enhanced adhesion. Similar research was conducted by Andrews and Young (1993) on discontinuous aramid fibers/epoxy model composites. They mapped the strain distribution along the fiber/matrix interphase by monitoring the band shift of the 1610 cm^{-1} peak, then calculated for the interfacial shear stress based on the strain profile. The positive effect of sizing treatments on the interfacial stress transfer was also discussed in their report.

Boogh *et al.* (1992) employed the Raman-tensile technique to study the stress transfer in high-performance epoxy composites reinforced with polyethylene (PE) fibers. After obtaining the calibration curve of asymmetric and symmetric C-C bands of PE fibers, they collected Raman spectra at different locations along the embedded PE fibers, and converted the band shift to the local axial strain of that fiber. Then the stress transfer length, defined as the length over which the stress reduces from maximum to zero, was determined. The researchers compared the stress transfer length of untreated PE fibers with that of plasma-treated fibers, and found that treated fibers had substantially shorter stress transfer length, indicating enhanced the interactions between the fibers and matrix.

Tze *et al.* (2007) evaluated the load transfer in cellulosic-fiber/polystyrene interphase by using a micro-Raman tensile test. They strained in tension a single fiber bonded with a micro-droplet of polymer and collected Raman spectra along the embedded region of the fiber. Based on the prior stress calibration of the 895 cm^{-1} band shift, the stress distribution in the fiber/polymer interphase was determined. Observation of the stress profile revealed that there was a transfer of load to the polymer as the fiber was strained. Additionally, different surface treatments of cellulose fibers generated different stress profiles at the fiber/polymer interphase, indicating that different interphases were created upon bonding with polystyrene.

2.5. Stress or load transfer measurement in nanocomposites using Raman spectroscopy

As Raman spectroscopy is a powerful tool to study the interfacial properties of composites, it has been employed to measure the efficiency of stress or load transfer from matrix materials to either synthetic or natural nano-sized fibers in the (nano)composites.

Carbon nanotubes are considered a promising candidate as a mechanical reinforcing agent in composite materials due to its outstanding mechanical properties. Its theoretical Young's modulus and tensile strength are as high as 5TPa and 200GPa, respectively (Cooper *et al.* 2001). The reinforcement efficiency of these nanotubes, however, varies depending on the efficiency of stress (or load) transfer between the nanotubes and matrix material. Schadler *et al.* (1998) observed, using Raman spectroscopy, the load transfer behavior of multi-walled carbon nanotube/epoxy composites in both tension and compression modes. The results showed that the 2700 cm^{-1} Raman peak shifted to higher

wavenumbers by a rate of $7cm^{-1}$/% compressive strain, but in tension, the shift is smaller, and it was toward higher wavenumbers. This shift behavior in tension loading contradicted the typical behavior of stress-sensitive Raman bands, which were reported in many studies to shift to lower wavenumbers. The atypical behavior was postulated to be due to difficulty in loading the nanotubes in tension, while it was easier to compress nanotubes oriented at an angle to the loading direction. The difference in Raman band shift between tension and compression was postulated to relate to the structure of multi-walled carbon nanotubes. It was proposed that in tension, load was transferred to the outer layer, but not effectively to the inner layers because of the relatively weak bonding between the nanotube layers. In compression, however, both outer and inner layers were deformed due to the seamless structure of the tubes and the geometrical constraint the outer layers imposed on the inner ones.

Later, Cooper *et al.* (2001) reported a Raman study of epoxy composites filled with either single-walled carbon nanotubes (SWNT) of two different preparing methods (pulsed-laser and arc-discharge) or multi-walled nanotubes (MWNT). Raman spectra were collected from the tension side of specimens subjected to a four-point bending. Results showed that the position of G' Raman band shifted significantly to a lower wavenumber upon tensile application, indicating the transfer of load from the matrix to the nanotubes.. The Raman band shift rate for SWNT prepared with pulsed laser was higher than that prepared with arc-discharge, which was believed to be a consequence of the low modulus and poor dispersion of the later SWNT, whereas the band shift rate for MWNT was between the two composite systems. A broadening of G' Raman peak was also observed,

possibly due to the random orientation of carbon nanotubes, with each alignment (with respect to the axis of composite deformation) affording a different efficiency of load transfer, thereby causing a less uniform molecular deformation which was reflected in the resultant Raman band.

Frogley *et al.* (2003) studied the mechanical properties of silicone based elastomers blended with single-walled carbon nanotubes. They observed an initial increased in modulus as a function of the applied strain, but at around 10-20% strain the enhancement effect vanished for all samples. In order to explain the "pseudo-yield" behavior of the composites, the authors employed Raman spectroscopy to study the process of stress transfer between nanotubes and the silicone rubber. The Raman study revealed a non-linear relationship of Raman band shift with tensile strain on the composite samples. Specifically, the Raman frequency decreased linearly with strain at first, then attained a constant value at about 50% strain, at which point stress was postulated to no longer being efficiently transferred to the nanotubes, thus explaining the "pseudo-yield" behavior at the macroscopic level. Mu *et al*. (2009) also observed a similar non-linear behavior in their Raman studies of stress transfer between poly (methylmethacrylate) (PMMA) and SWNT. A high efficiency of load transfer to the SWNT was observed within a range of low composite strain (less than 0.2%), which was accompanied by an elastic deformation. But at high strain levels, slippage took place at the SWNT-PMMA interphase and load transfer ceased to occur. Based on the results, a conclusion was made that the maximum load transfer was limited by fiber/matrix adhesion, which controlled the overall improvement of the mechanical properties of nanocomposites.

In order to promote the interfacial adhesion between carbon nanotubes and the matrix polymer, many surface modification methods were proposed for the nano-fiber, and the effectiveness of these methods were verified from the load transfer ability using Raman spectroscopy. Liu et al. (2005) prepared poly (vinyl alcohol) (PVA) nanocomposites with SWNT functionalized with hydroxyl groups for an enhanced fiber/matrix compatibility. The researchers compared the shift of D* Raman band of functionalized SWNT with that of the control samples. The rate of stress transfer from the matrix to the nanotubes was determined from the slope of Raman band shift with respect to the applied strain of the composite samples. The results showed a larger slope in the case of functionalization (as opposed to no treatment), suggesting that a higher stress was transferred across the compatibilized interphase at a given level of applied strain.

Eitan *et al*. (2006) also studied the effect of MWNT surface modification on the efficiency of stress transfer between nanotubes and polycarbonate (PC) using Raman spectroscopy. PC nanocomposite filled with either epoxide-modified MWNT or untreated nanotubes were mechanically deformed and subjected to Raman spectra collection to monitor the position of the second order disorder peak. The band shifted more abruptly as a function of applied strain for PC filled with epoxide-treated MWNT, hence suggesting a higher efficiency of load transfer compared to the untreated nanotubes. Wang *et al.* (2008) compared two different surface modification methods for carbon nanotubes by using Raman spectroscopy. They found that the epoxide-grafted carbon nanotubes exhibited a more significant shift of the Raman G band compared to the

amino-grafted nanotubes. The higher band shift was also validated by the higher bulk mechanical properties of the epoxide-nanotube filled composites.

Besides synthetic nano fibers, natural nano-fibers especially nano-sized cellulose, has been increasingly studied for polymer reinforcement not only because of its promising mechanical properties but also its abundance, renewability and biodegradability. There are, however, only few reported studies about using Raman spectroscopy to examine the transfer of load between cellulosic nano-fibers and the matrix in the composite. Of the few studies, Šturcová et al. (2005) examined the stress-transfer properties of epoxy composites containing tunicate cellulose whiskers that are about 15nm in diameter. The researchers deformed the samples using a 4-point bending test, analyzed the shift of the Raman band at 1095 cm^{-1}, and plotted the shifts with respect to the applied strain of composites. The peak shift was found to linearly dependent on the applied strain up to about 0.8%, but plateau at higher strain values. The peak shift was considered an indication of epoxy-to-whisker stress transfer, which resulted in a direct stressing (or straining) of the molecular backbone of cellulose. The peak shift plateau was thought to reflect a decreased efficiency of stress transfer between the constituent components in the composites, possibly due to the weakening or debonding at the whisker-matrix interphase.

Quero *et al.* (2009) also employed Raman spectroscopy to evaluate the stress transfer efficiency in bacterial cellulose (BC)/poly(L-lactic acid) (PLLA) composites. In order to optimize the mechanical performance of the composites, they embedded two forms of BC network, cultured for 3 days and 6 days, into PLLA matrix. Samples were stressed in

tension while Raman spectra were collected at each strain level to follow the molecular deformation of the samples by monitoring the Raman band shifts at 1095 cm^{-1}. Results showed that at a given applied strain (or stress) level, the band shift was higher for the BC networks cultured for 3 days than for 6 days. The inferred lower efficiency of load transfer was thought to be a result of the laminated structure of the 6-day culture, leading to a less efficient interphase.

Based on the aforementioned review, it can be inferred that interfacial properties of biobased nanocomposites are under studied. Moreover, Raman spectroscopy, which has been proven useful in assessing the load transfer ability in carbon nanotube composites, has rarely been used to study cellulose nanocomposites. Therefore, it is duly justified to conduct Raman studies of load transfer in nano-cellulose filled polymers especially biopolymer such as poly(lactic acid).

2.6. References

Andrews MC, Young RJ (1993) Analysis of the deformation of aramid fibres and composites using raman spectroscopy. Journal of Raman Spectroscopy 24(8):539-544.

Barber AH, Cohen SR, Eitan A, Schadler LS, Wagner HD (2006) Fracture transitions at a carbon-Nanotube/Polymer interface. Advanced Materials 18(1):83-87.

Barber AH, Cohen SR, Kenig S, Wagner HD (2004) Interfacial fracture energy measurements for multi-walled carbon nanotubes pulled from a polymer matrix. Composites Science and Technology 64(15):2283-2289.

Barber AH, Cohen SR, Wagner HD (2003) Measurement of carbon nanotube--polymer interfacial strength. Applied Physics Letters 82(23):4140-4142.

Boogh LCN, Meier RJ, Kausch H, Kip BJ (1992) A raman microscopy study of stress transfer in high-performance epoxy composites reinforced with polyethylene fibers. Journal of Polymer Science Part B: Polymer Physics 30(4):325-333.

Cheng T-, Jones FR, Wang D (1993) Effect of fibre conditioning on the interfacial shear strength of glass-fibre composites. Composites Science and Technology 48(1-4):89-96.

Cooper CA, Young RJ, Halsall M (2001) Investigation into the deformation of carbon nanotubes and their composites through the use of raman spectroscopy. Composites Part A: Applied Science and Manufacturing 32(3-4):401-411.

Cooper CA, Cohen SR, Barber AH, Wagner HD (2002) Detachment of nanotubes from a polymer matrix. Applied Physics Letters 81(20):3873-3875.

Davies RJ, Montes-MorÃ ¡n MA, Riekel C, Young RJ (2001) Single fibre deformation studies of poly(p-phenylene benzobisoxazole) fibres part I determination of crystal modulus. Journal of Materials Science 36(13):3079-3087.

Day RJ, Robinson IM, Zakikhani M, Young RJ (1987) Raman spectroscopy of stressed high modulus poly(p-phenylene benzobisthiazole) fibres. Polymer 28(11):1833-1840.

Drzal LT, Madhukar M (1993) Fibre-matrix adhesion and its relationship to composite mechanical properties. Journal of Materials Science 28(3):569-610.

Eichhorn SJ, Bennett JA, Shyng YT, Young RJ, Davies RJ (2006) Analysis of interfacial micromechanics in microdroplet model composites using synchrotron microfocus X-ray diffraction. Composites Science and Technology 66(13):2197-2205.

Eichhorn SJ, Sirichaisit J, Young RJ (2001a) Deformation mechanisms in cellulose fibres, paper and wood. Journal of Materials Science 36(13):3129-3135.

Eichhorn SJ, Young RJ, Yeh W- (2001b) Deformation processes in regenerated cellulose fibers. Textile Research Journal 71(2):121-129.

Eitan A, Fisher FT, Andrews R, Brinson LC, Schadler LS (2006) Reinforcement mechanisms in MWCNT-filled polycarbonate. Composites Science and Technology 66(9):1162-1173.

Frogley MD, Ravich D, Wagner HD (2003) Mechanical properties of carbon nanoparticle-reinforced elastomers. Composites Science and Technology 63(11):1647-1654.

Ganesan Y, Lou J (2009) The mechanical characterization of carbon-nanotube-reinforced polymer-matrix nanocomposites: An unfolding story of interface. JOM Journal of the Minerals, Metals and Materials Society 61(1):32-37.

Gierlinger N, Schwanninger M, Reinecke A, Burgert I (2006) Molecular changes during tensile deformation of single wood fibers followed by raman microscopy. Biomacromolecules 7(7):2077-2081.

Hamad WY, Eichhorn S (1997) Deformation micromechanics of regenerated cellulose fibers using raman spectroscopy. Journal of Engineering Materials and Technology 119(3):309-313.

Herrera-Franco PJ, Drzal LT (1992) Comparison of methods for the measurement of fibre/matrix adhesion in composites. Composites 23(1):2-27.

Hwang GL, Shieh Y-, Hwang KC (2004) Efficient load transfer to polymer-grafted multiwalled carbon nanotubes in polymer composites. Advanced Functional Materials 14(5):487-491.

Kelly A, Tyson WR (1965) Tensile properties of fibre-reinforced metals: Copper/tungsten and copper/molybdenum. Journal of the Mechanics and Physics of Solids 13(6):329-338, in1-in2, 339-350.

Kim JK. (1998) Engineered interfaces in fiber reinforced composites Elsevier Science Ltd, Burlington.

Kim J-, Zhou L, Mai Y- (1993) Stress transfer in the fibre fragmentation test: Part I an improved analysis based on a shear strength criterion. Journal of Materials Science 28(22):6233-6245.

Leeuw TK, Tsyboulski DA, Nikolaev PN, Bachilo SM, Arepalli S, Weisman RB (2008) Strain measurements on individual single-walled carbon nanotubes in a polymer host: Structure-dependent spectral shifts and load transfer. Nano Letters 8(3):826-831.

Liu L, Barber AH, Nuriel S, Wagner HD (2005) Mechanical properties of functionalized single-walled carbon-Nanotube/Poly(vinyl alcohol) nanocomposites. Advanced Functional Materials 15(6):975-980.

Liu T, Tong Y, Zhang W (2007) Preparation and characterization of carbon nanotube/polyetherimide nanocomposite films. Composites Science and Technology 67(3-4):406-412.

Miller B, Gaur U, Hirt DE (1991) Measurement and mechanical aspects of the microbond pull-out technique for obtaining fiber/resin interfacial shear strength. Composites Science and Technology 42(1-3):207-219.

Mitra VK, Risen J,William M., Baughman RH (1977) A laser raman study of the stress dependence of vibrational frequencies of a monocrystalline polydiacetylene. The Journal of Chemical Physics 66(6):2731-2736.

Mu, Minfang, Sebastian Osswald, Yury Gogotsi, and Karen I. Winey. 2009. An in situ raman spectroscopy study of stress transfer between carbon nanotubes and polymer. Abstract. *Nanotechnology* 20, no. 33:335703.

Paipetis A, Galiotis C (1996) Effect of fibre sizing on the stress transfer efficiency in carbon/epoxy model composites. Composites Part A: Applied Science and Manufacturing 27(9):755-767.

Qian D, Dickey EC, Andrews R, Rantell T (2000) Load transfer and deformation mechanisms in carbon nanotube-polystyrene composites. Applied Physics Letters 76(20):2868-2870.

Quero F, Nogi M, Yano H, Abdulsalami K, Holmes SM, Sakakini BH, Eichhorn SJ (2009) Optimization of the mechanical performance of bacterial Cellulose/Poly(l-lactic) acid composites. ACS Applied Materials & Interfaces.

Robinson IM, Zakikhani M, Day RJ, Young RJ, Galiotis C (1987) Strain dependence of the raman frequencies for different types of carbon fibres. Journal of Materials Science Letters 6(10):1212-1214.

Roman I, Aharonov R (1992) Mechanical interrogation of interfaces in monofilament model composites of continuous SiC fiber-aluminum matrix. Acta Metallurgica Et Materialia 40(3):477-485.

Schadler LS, Giannaris SC, Ajayan PM (1998) Load transfer in carbon nanotube epoxy composites. Applied Physics Letters 73(26):3842-3844.

Schultz J, Lavielle L, Martin C (1987) The role of the interface in carbon fibre-epoxy composites. The Journal of Adhesion 23(1):45.

Shyng Y, Bennett J, Young R, Davies R, Eichhorn S (2006) Analysis of interfacial micromechanics of model composites using synchrotron microfocus X-ray diffraction. Journal of Materials Science 41(20):6813-6821.

Shyng YT, Eichhorn SJ, Young RJ, Davies RJ (2007) Investigation of interfacial stress transfer in a PBO/polypropylene microdroplet composite using synchrotron microfocus X-ray diffraction. Composite Interfaces 14(4):351-359.

Sturcova A, Davies GR, Eichhorn SJ (2005) Elastic modulus and stress-transfer properties of tunicate cellulose whiskers. Biomacromolecules 6(2):1055-1061.

Tripathi D, Jones FR (1998) Single fibre fragmentation test for assessing adhesion in fibre reinforced composites. Journal of Materials Science 33(1):1-16.

Tze W, O'Neill S, Tripp C, Gardner D, Shaler S (2007) Evaluation of load transfer in the cellulosic-Fiber/Polymer interphase using a micro-raman tensile test. Wood and Fiber Science 39(1):184-195.

Wagner HD, Lourie O, Feldman Y, Tenne R (1998) Stress-induced fragmentation of multiwall carbon nanotubes in a polymer matrix. Applied Physics Letters 72(2):188-190.

Wagner HD, Vaia RA (2004) Nanocomposites: Issues at the interface. Materials Today 7(11):38-42.

Wang S, Liang R, Wang B, Zhang C (2008) Load-transfer in functionalized carbon nanotubes/polymer composites. Chemical Physics Letters 457(4-6):371-375.

Young RJ, Day RJ, Zakikhani M (1990) The structure and deformation behaviour of poly(p-phenylene benzobisoxazole) fibres. Journal of Materials Science 25(1):127-136.

Young RJ, Eichhorn SJ, Shyng Y, Riekel C, Davies RJ (2004) Analysis of stress transfer in two-phase polymer systems using synchrotron microfocus X-ray diffraction. Macromolecules 37(25):9503-9509.

Chapter 3 Design of a micro-tensile testing system

3.1.Chapter summary

Considering load (less than 200g) and space limits (less than 15cm by 15cm) of the X-Y stage of the Raman microscope, a low-profile tensile testing system was built up to hold and stretch samples under the Raman microscope. In this system, a miniature tensile stage was designed and fabricated to meet the requirement of the X-Y stage. A servo motor actuates linear movement of this stage. A miniature load cell mounted on this stage was used to sense stress information on specimens, which was digitalized by a data acquisition device and transmitted to a computer. This tensile system was automated by a user interface developed by a graphical programming platform called LabVIEW. The performance of this system was evaluated where low non-linearity and insignificant systematic errors were obtained in the calibration section.

3.2. Introduction

In this chapter, the design of a micro-tensile testing system is described for Raman/tensile tests of composites samples. Figure 3.1 shows the configuration diagram of this testing system. This system consists of three parts: mechanical, electronic, and software.

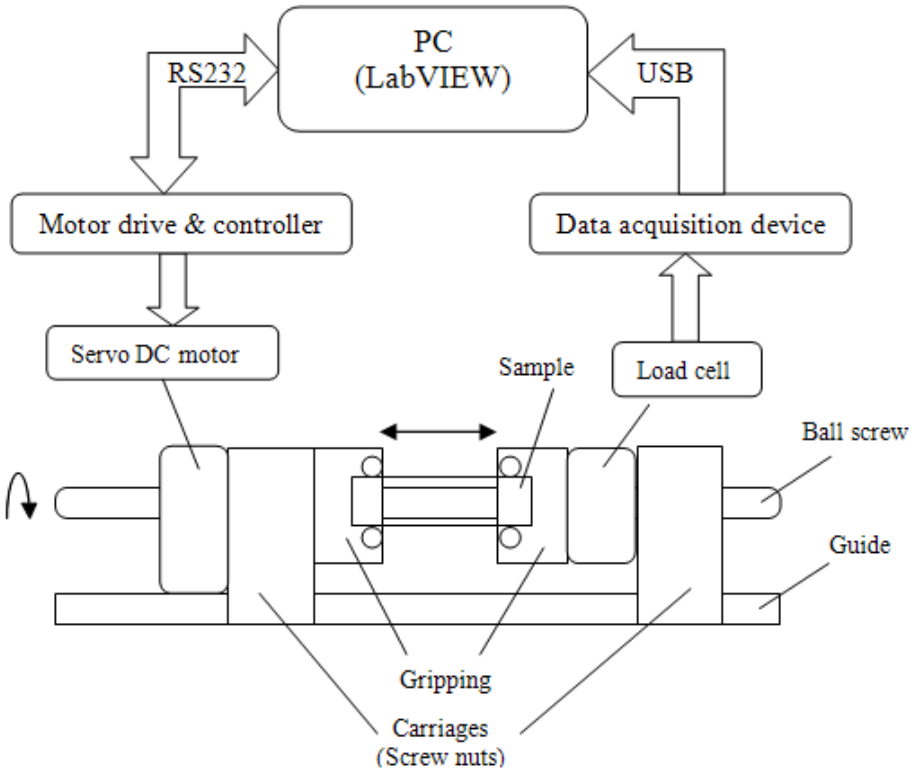

Figure 3.1 Configuration diagram of the micro-tensile testing system

Considering load (less than 200g) and space limits (less than 150cm by 150cm) of the X-Y stage of the Raman microscope, a miniature tensile testing stage was designed and fabricated to hold and stretch composite samples under the Raman microscope. When the stage stretches a sample, a load cell senses the load information on the sample and converts it into electrical signals, and then a data acquisition device digitalizes and transmits these signals to a computer via a USB cable. A servo DC motor actuates the

linear motion of this stage. A user interface program on the computer implements the control of the system and data recording.

3.3. Mechanical part

The mechanical part of this micro-tensile testing system includes a ball screw assembly, two gripping clamps, a linear guide, two carriages, and a load cell (Figure 3.1).

The ball screw assembly is the main part of this tensile testing stage, which converts the motor's rotary motion into a linear motion (Figure 3.2). Different from a lead screw assembly, a ball screw assembly utilizes a series of bearing balls between the screw and nut to improve the screw mechanical efficiency and wear life. The ball screw in this design is fabricated as a bi-directional profile so that the screw nuts can simultaneously move towards two opposite directions when the motor turns. The bi-directional profile in this design is to keep the mid-span of the specimen in the center for repeated spectra collection as the stretching progresses.

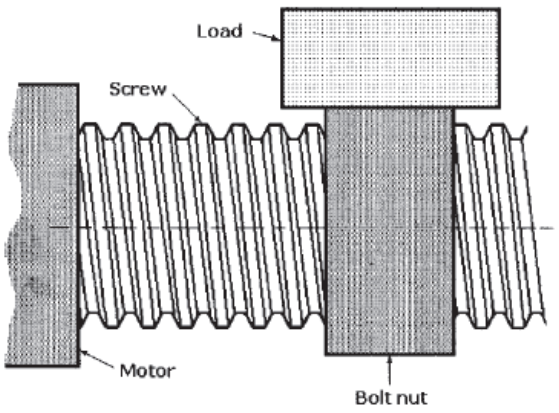

Figure 3.2 Ball screw assembly mechanism (Sclater and Chironis 2001)

The linear guide supports the mass of the load and assures smooth, straight-line motion while minimizing friction. The gripping parts hold and secure the sample on the stage, and four screws are fastened at the gripping clamps to prevent the sample from slipping. Two carriages connecting the screw nuts and the linear guide support the gripping clamps and the load cell. One of the carriages has two slots so that two load cells can be mounted and measure tension and compression forces respectively.

The Honeywell Model 13 subminiature load cell is used as the force transducer. The load cell has a single diaphragm construction with a maximum measureable load of 50 lb, an accuracy of 0.7 % and a weight of 1 gram. A balance module containing "dummy" gauges is also included in the load cell's lead wire cable to fulfill a Wheatstone bridge circuit for temperature compensation.

3.4. Electronic part

There are two components in the electronic part: a servo control system and a data acquisition device (Figure 3.1). The servo control system consists of a DC motor, a planetary gearhead, a magnetic encoder and a motor controller. In view of the lightweight requirement, a miniature DC servomotor system provided by MicroMo Electronics, Inc is used as the servo control system.

In this system, a coreless DC motor 1516A012SR is used to provide the rotary motion. The features of the coreless DC motor include no cogging, no iron losses, extremely low current consumption, low starting voltage, low rotor inertia and extremely light and compact profile.

The coreless DC motor alone cannot supply adequate torque for the micro-tensile stage. A gearhead that converts high-speed, low-torque rotary motion to a low-speed, high-torque output is mounted directly to the coreless motor. The gearhead 15A with a reduction ratio of 152:1 and 150 mNm continuous output torque is employed as the speed-torque converter.

To achieve an accurate control of motor velocity and position, an encoder as the feedback sensor is needed in the closed-loop servo system. An integral magnetic encoder IE2 – 512 is used to provide feedback signals for the servomotor. This encoder, with512 lines per revolution, is integrated into the DC motor 1516A012SR, and the addition extends the overall length by only 1.4 mm.

The motor controller, as the “brain” of a servo control system, executes all the calculation required for motion path planning and servo-loop closure. It also receives operational instructions from the user interface in the computer and responses with corresponding command signals for the motor driver that controls the DC motor. MCDC 3006S is used to control the servomotor. This controller is designed to achieve velocity, position and torque control with RS232 interface to computers and other controllers. There is also an ASCII command set available for programming.

Two issues need addressing before load information can be recorded in the computer. The electrical signals converted by the load cell from forces on samples are too small. In addition, signals from the load cell are analog signals that cannot be stored in computers.

Hence, a data acquisition device that can amplify and digitalize signals from the sensor becomes the other component of the electronic part in the micro-tensile testing system.

Considering the excitation voltage of the load cell and portability requirement, National Instruments 9237 is used as the data acquisition device. NI 9237 is a 4-channel bridge module designed to implement load cell measurement. It has 24-bit resolution on four simultaneous inputs sampled at up to 50k sample/second/channel and up to 10V programmable excitation. Figure 3.3 shows the wiring full-bridge configuration of NI 9237.

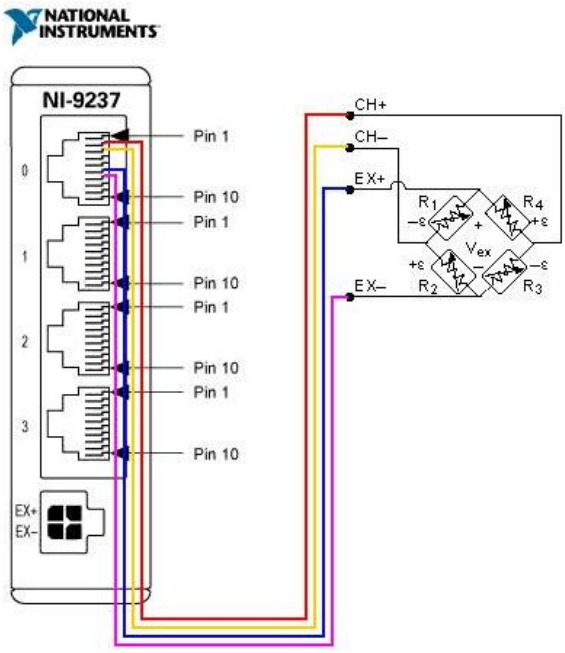

Figure 3.3 Wiring in full-bridge configuration (http://zone.ni.com/devzone/cda/tut/p/id/7138, accessed on June 15, 2010)

3.5. User interface design

The user interface provides operators a terminal where all the functions of the micro-tensile testing system are integrated. Through the user interface, operators can input

experiment parameters for tensile and stress relaxation tests, observe real-time data trend, control velocity, motion direction and displacement of the tensile stage, and save test results on the computer.

LabVIEW from National Instruments is employed as the development platform for the user interface design. LabVIEW is a visual programming language that enables users to create programs by using intuitive graphical icons and wires that resemble a flowchart. This feature accelerates prototyping and development of the program. Another advantage of LabVIEW is its integrated access to plenty of hardware devices, including the data acquisition device used in the micro-tensile testing system.

There are two parts in the user interface of the micro-tensile testing system: the front panel and the block diagram. In the front panel, operators can set up specific experiments by inputting corresponding parameters and observing experiment results and system operating states from certain display areas. In the block diagram, all the functions of the front panel are implemented by assembled data flowchart using graphical icons and wires.

Figure 3.4 shows a screenshot of the front panel developed for the micro-tensile testing system. There are three areas in the front panel: data display area, instrument control area and operating state indicator area.

In the data display area, operators can monitor load information with respect to time and displacement of the tensile stage in two charts: "Load vs. Time" and "Load vs. Displacement".

In the instrument control area, users can control the tensile stage by clicking buttons in this area. There are three tags in the left part of this area: motion control, tensile test setup and stress relaxation test setup. In the motion control tag, the operator can adjust the distance between two gripping clamps, set a homing position and return to the last homing position. Through the other two tags, tensile and stress relaxation tests can be set up by entering experiment parameters. In the right part of this area, operators can stop signal reading from the load cell, interrupt current test, and choose a file path to save test data.

In the operating state indicator area, signal lights with different colors will inform users of the current operating state of the micro-tensile testing system, such as “Homing set”, “Stop”, “Testing” and “Error”.

The function of each button and indicator is summarized in Table 3.1.

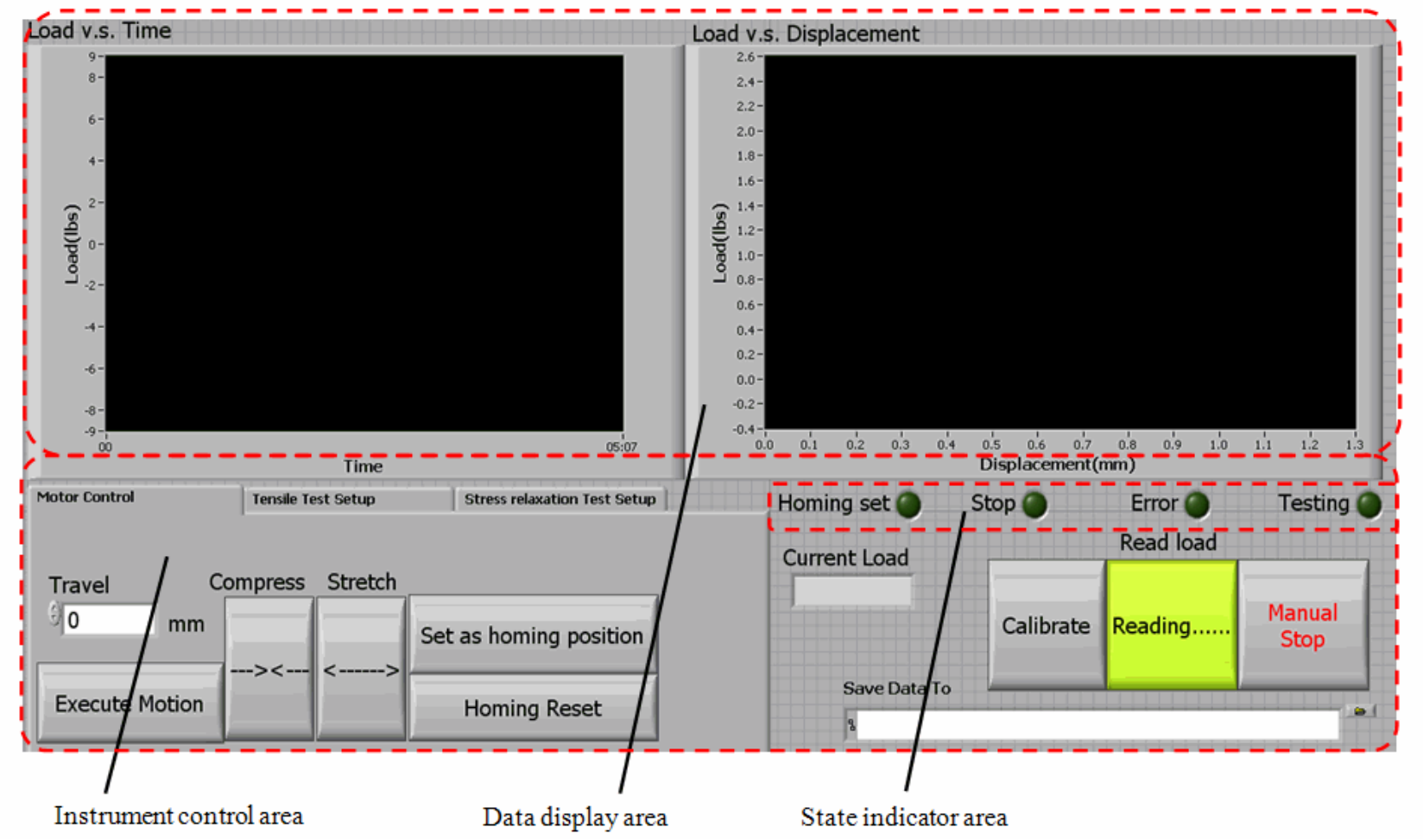

Figure 3.4 Screenshot of the user interface

Table 3.1 Function list of the user interface

Name	Submenu	Function
Load vs. Time		*Display load trend with respect to time*
Load vs. Displacement		*Display load trend with respect to displacement*
Motion control	Travel	*Specify the distance the two gripping clamps will travel*
	Execute motion	*Execute the motion specified in Travel*
	Compress	*Execute compressive motion*
	Stretch	*Execute stretching motion*
	Set as homing position	*Set current position as a homing position*
	Homing reset	*Return to the last homing position*
Tensile test setup	Span	*Specify the distance between the two gripping clamps*
	Extension	*Specify the distance the clamps will travel in terms of percentage of the span*
	Test speed	*Specify the speed of the test*
	Start test	*Execute tensile test*
Stress relaxation test setup	Span	*Specify the distance between the two gripping clamps*
	Time interval after stretch	*Specify the time interval after each stretch*
	Extension per stretching	*Specify the distance the clamps will travel in each stretch in terms of percentage of the span*
	Stretch speed	*Specify the speed of each stretching*
	NO. of stretching	*Specify the number of stretching*
	Start test	*Execute stress relaxation test*
Homing set		*Indicate if a homing position has been set*
Stop		*Indicate if the two clamps are paused*
Error		*Indicate any error in the system*
Testing		*Indicate if any test is running*
Current load		*Display current load*
Calibrate		*Calibrate the load cell*
Read load		*Stop reading load from the load cell*
Manual stop		*Interrupt a current running test*
Save data to		*Specify a path for saving the test data*

Figure 3.5 shows the structure of the block diagram of the micro-tensile testing system. After starting the user interface, the program first enters the initialization stage where the user interface communicates with the motor controller and the data acquisition device and checks if those devices are plugged in and functioning properly, and then initializes those devices with specific parameters. During this stage, the program also sets all the indicators and display windows as the default state.

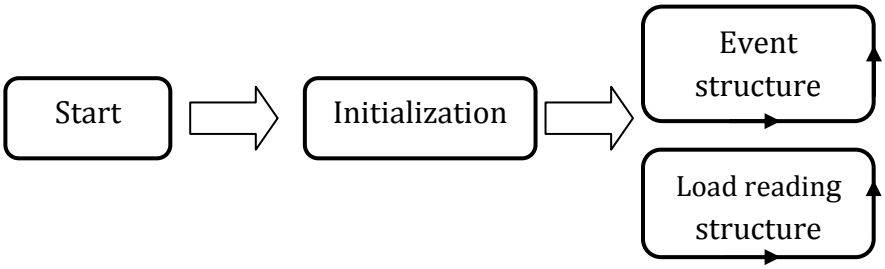

Figure 3.5 Block diagram structure

After initializing the user interface, the program goes to two parallel loop structures: event structure and load reading structure. The load reading structure updates load information on the tensile stage recorded from the load cell. The event structure monitors the control buttons in the front panel and responds to user's input on the front panel. There are eight subroutines corresponding to eight control buttons on the front panel.

Table 3.2 lists the name and the corresponding control buttons of the eight subroutines. Refer to Table 3.1 for the function of each control buttons.

Execution of each subroutine will switch on or off certain signal lights in the state indicator area in the front panel to inform the user a task is either still running or has been

completed. For example, after clicking the “Start Test” on the “Tensile Test Setup” tag, the “Tensile Test” subroutine will turn on the “Testing” light. Then when the tensile test is finished, the subroutine will turn off the “Testing” light, and turn on the “Stop” light to signal the user the test is done and the tensile stage is currently not moving.

During execution of any one subroutine, the other subroutines are not available to operators to ensure the current subroutine completes the task without being interrupted.

Table 3.2 Subroutines in the event structure

Name	Corresponding control buttons
Compress	---><---
Stretch	<------>
Execute motion	Execute Motion
Set as homing position	Set as homing position
Homing	Homing Reset
Calibration	Calibrate
Tensile test	Start Test
Stress relaxation test	Start Test

3.6. Calibration

To verify the performance of the micro-tensile testing system, the output distance between the two gripping clamps of the system is measured by a vernier caliper and compared to the commanded input distance.

The non-linearity of the system evaluates the degree to which a system can maintain a linear relationship between the input and the output. It is defined as the maximum

deviation (B) of the input-output curve from a fitted straight line over a defined range (A):

$$\text{Nonlinearity} = B/A \times 100\% \qquad (3.1)$$

For the micro-tensile testing system, the non-linearity was measured within a range of 10mm to 50 mm of the distance between the two clamps with a speed of 7.5 mm/min. The fitted line was obtained by using least squares of the error between the input and the output distance. Figure 3.6 plots the scatter data of input and output distances and the fitted straight line. According to the definition of 3.1, the nonlinearity of the system is 0.1392%.

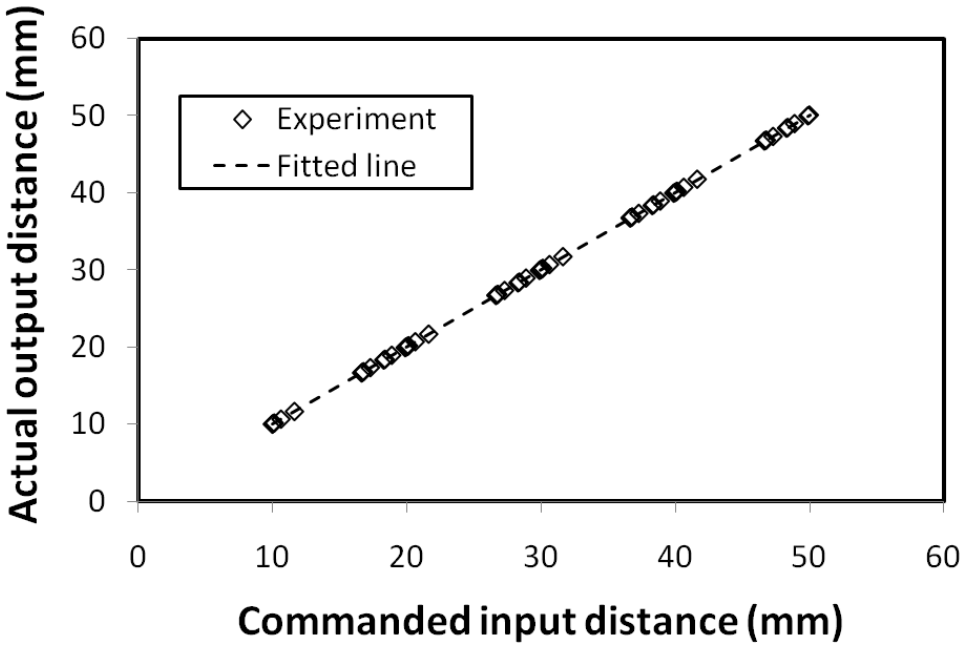

Figure 3.6 Scatter chart of the input and output distance with least squares fitted line.

The error of the system was also evaluated in three different speeds of 0.5mm/min, 1.0mm/min and 1.5mm/min. The commanded input distances were compared to the

output distance. The difference between input and output distance was plotted. These errors are randomly distributed around zero without observable trend as seen in Figure 3.7, which indicates that the error of the system is dominated by random errors and systematic error is not significant.

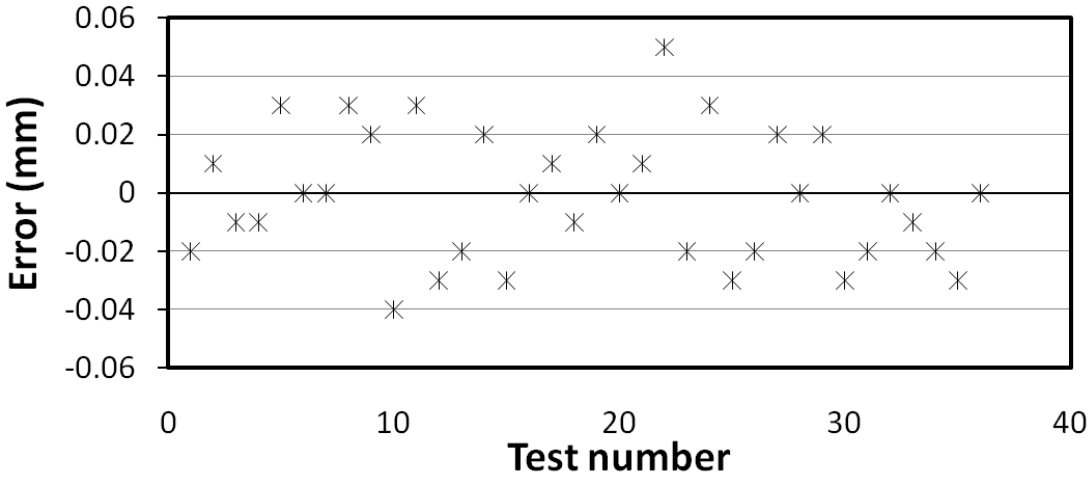

Figure 3.7 Error distribution of the micro-tensile testing system.

3.7. Conclusion

In this chapter, the design of the micro-tensile testing system was described for Raman/tensile tests on composites. The implement and function of each component in this testing system were provided and illustrated in detail. Finally, the performance of this system was evaluated where low non-linearity and insignificant systematic errors were obtained in the calibration section.

3.8. References

Sclater N, Chironis NP (2001). Mechanisms and Mechanical Devices Sourcebook (3rd Edition). (pp: 5). McGraw-Hill. (http://knovel.com/web/portal/browse/display?_EXT_KNOVEL_DISPLAY_bookid=659&VerticalID=0, accessed on June 15, 2010)

Chapter 4 Raman spectroscopic studies of nano-cellulose-filled poly(lactic acid) composites – spectral analysis

4.1.Chapter summary

Raman spectroscopy was employed to study the load transfer to nano cellulose fibers (microfibrillated cellulose) in composites of poly(lactic acid) resin. A protocol was established to standardize experimental procedures. This accuracy of this protocol was also verified for discussion of the interfacial adhesion effect. This protocol includes techniques of spectrum collecting and processing to isolate the Raman band of cellulose for frequency shift analysis. Preliminary results obtained using this protocol was also discussed.

4.2.Introduction

Polylactide (PLA) or polylactic acid, derived from sugar (e.g. of corn starch and sugarcanes), is a promising thermoplastic polyester because of its renewable resource-based origin along with its biodegradability and biocompatibility (Ragauskas *et al.* 2006). It is an attractive sustainable alternative to certain petroleum-based polymers, such as polyolefin. However, the inherent brittleness of PLA has been a major drawback for its large-scale commercial applications (Bhardwaj and Mohanty 2007). Increasing attempts are made to reinforce mechanically disadvantaged bioplastics by incorporating high-performance fibers in PLA matrix. Among many avenues of producing composites, preparation of bionaoncomposites has become an attractive approach because of the renewability and biodegradability of both material matrix and reinforcement (Oksman *et al.* 2006), and also the high efficiency of nano-scale reinforcement of matrix materials.

One of the candidates as reinforcing agents for PLA matrix is mechanically isolated cellulose microfibrils, known as microfibrillated cellulose (MFC) with a dimensional distribution down to nanoscale (Herrick *et al.* 1983). Two features of MFC are, (1) exceptionally large specific surface area, implying its potentially high capacity to interact with secondary components/materials (Stenstad *et al.* 2008), and (2) highly accessible by cellulase enzyme (Herrick *et al.* 1983), implying its biodegradability. These two outstanding features of MFC indicate that the surface chemistry of this stiff nano-cellulose can be potentially tuned to interact favorably with PLA to enhance mechanical properties of the bioplastic while maintaining its biodegradation advantage.

To evaluate the effectiveness of reinforcement on matrix, it is important to achieve an improved understanding of the factors that influence the mechanical properties of biocomposites. Such factors include properties of the reinforcing agent, the matrix polymer, and the interphase, as well as the distribution behavior of reinforcing medium in the matrix (Hoecker and Karger-Kocsis 1996). Among these properties in composites, interphase, especially stress/load transfer between reinforcement and matrix, has been drawing much attention in terms of its role in improving the mechanical properties of the matrix.

Many techniques have been developed to measure the stress/load transfer ability in composites with different reinforcing agents down to nano-scale. Schultz *et al.* (1987) utilized fiber fragmentation tests to evaluate the effect of oxidization treatment on the ability of the interface to transfer stress from the epoxy to the carbon fibers. This method has been limited by the lack of an accurate data reduction technique (Tripathi and Jones 1998). Synchrotron microfocus X-ray diffraction was employed to study the stress transfer mechanism in two-phase polymer systems (Young *et al.* 2004). However, this technique may not be used to study the stress transfer mechanism in composite systems reinforced with fibers of low crystallinity because of difficulty in acquiring well-defined X-ray diffraction patterns. In addition, X-ray induced radiation damage potentially limits the application of this technique.

In the studies of nano-scale reinforcement in composites, examination of the ability to transfer load (or stress) between nano fibers and matrix relies on classical bulk mechanical tests complemented with microscopic qualitative analyses. Hwang *et al.*

(2004) employed *in situ* transmission electron microscopy (TEM) to provide supportive information about the efficiency of load transfer between carbon nanotube grafted with poly(methyl methacrylate) (PMMA) and commercial PMMA matrix. Under TEM, the tensile load was induced by charge accumulation, resulting in cracks bridged by carbon nanotubes. During the propagation of the crack, the carbon nanotube was gradually pulled out from the matrix, a qualitative analysis of the load transfer between the nanotube and the matrix was consequently obtained.

Raman spectroscopy has been utilized to study load (or stress) transfer mechanism since Raman peak of high-performance fiber was found to linearly shift towards lower frequencies with elongation (Mitra *et al.* 1977). Cellulose fibers have also been reported to exhibit a similar behavior upon application of external load (Hamad and Eichhorn 1997). Based on this knowledge, the transfer of load within cellulose-filled composite can be discerned by monitoring the frequency shift of stress-sensitive Raman band of cellulose fibers. This technique was recently applied to cellulose nanocomposites to study load transfer from PLA to bacterial cellulose nanofibers (Quero *et al.* 2009). It was revealed that nanofibers of higher surface areas (3-day culture) exhibited a higher PLA-to-cellulose load transfer than nanofibers of lower surface areas (6-day culture).

In the present study, Raman microscopy was employed to study the load transfer to nano cellulose fibers in composites of PLA resin. The objective of this chapter is to establish a protocol to standardize experimental procedures and to verify the accuracy of this protocol for discussion of the interfacial adhesion effect in the next chapter. This protocol includes techniques of spectrum collecting and processing to isolate the Raman band of

cellulose for frequency shift analysis. Preliminary results obtained using this protocol will also be discussed.

4.3.Materials and methods

PLA of injection-molding grade (3051D) was acquired from NatureWork LLC. Microfibrillated cellulose (MFC), prepared from high-pressure delamination of bleached wood pulp fibers, was obtained from the University of Maine Forest Bioproducts Research Initiative. The MFC was reacted with lactide at 180 ^{o}C for 1 hour. 0.5 dry-wt % modified MFC was blended into a PLA solution before being cast into a film. For comparisons, the same amount of untreated MFC was used to form the control sample. All composite films were prepared by the research group of Professor John Simonsen (Oregon State University) with whom we have an ongoing collaborative project funded by USDA (National Research Initiative grant no. 2008-35504-19158).

The composite film was glued with a fast-curing epoxy on a home-made mini tensile stage at least 24 hours before each test. During the test, the tensile stage, placed under a confocal Raman microscope (WITec alpha300 R), stretched the sample with an incremental strain of 0.5% at a speed of 7.5 mm/min. After each stretch, the film was held in position for spectra collection. This process was repeated up to a maximum strain value of 2%.

The confocal Raman microscope was equipped with an Ar-ion laser of 514.5 nm and polarized along the strain axis of the tensile stage. After the laser was focused onto a selected area of the composite film using a Nikon 10x objective (0.3 numerical aperture),

the spectrum was obtained in the backscattering geometry with a laser power of 35 mW. Since the exposure time for a single scan was 6 s, and the number of scans accumulated in each spectrum was 40 times, the total time was 4 min for a single spectrum.

The tensile stage was automated by a servo DC motor and controlled by a graphical user interface platform developed with LabVIEW. The load exerted to the sample was sensed by a load cell with a maximum measureable load of 50 lb and an accuracy of 0.7% full scale. The load was automatically recorded by a data acquisition device from National Instruments. The width and thickness of the sample were measured by a caliper.

4.4. Results and discussions

4.4.1 Spectrum processing

Load-sensitive Raman bands of cellulose have been identified at 1095 cm^{-1} and 895 cm^{-1} in regenerated cellulose fibers (Hamad and Eichhorn 1997), both of which shift linearly towards lower wavenumbers with the application of tensile stress or strain. 1095 cm^{-1} Raman band is corresponding to the cellulose C-O ring stretching modes (Wiley and Atalla 1987) with an alternative assignment for the glycosidic linkage (C-O-C) mode (Edwards *et al.* 1997) in Figure 4.1. 895 cm^{-1} Raman band has been assigned to mixed modes (C-C-C, C-H-O) including angle bending respectively (Wiley and Atalla 1987) in Figure 4.1. Both bands were observed in the Raman spectrum of MFC (Figure 4.2). In this research, we only analyzed the peak shift of 1095 cm^{-1} as its relatively high intensity in the spectrum reflects molecular deformation of cellulose polymer backbone chain where most of tensile forces are distributed. The wavenumber shift rate of this band has also

been reported invariant with stress (cm^{-1}/GPa) for both regenerated and natural cellulose fibers, such as flax and hemp fibers (Eichhorn *et al.* 2001a).

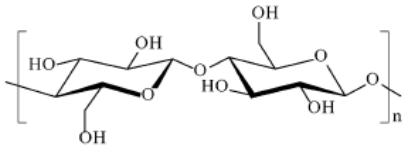

Figure 4.1 Structure of a cellobiose repeat unit for cellulose (Eichhorn *et al.* 2005)

Another reason for choosing 1095 cm^{-1} peak for analyzing band shift is from the comparison of Raman spectrum of neat PLA with that of MFC. In the spectrum of PLA (Figure 4.2), there is a very intense peak at a wave number slightly lower than 895 cm^{-1}, which may overwhelm the intensity of 895 cm^{-1} from MFC in the composite spectrum, considering the low weight loading of the nano-cellulose in composite samples.

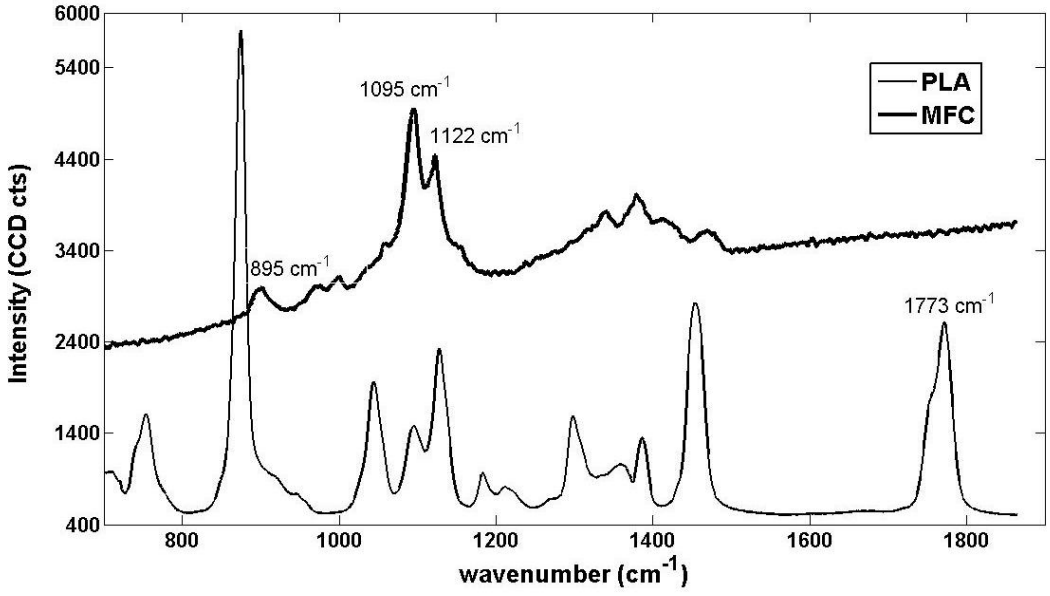

Figure 4.2 Raman spectrum of PLA and MFC (700 – 1900 cm^{-1})

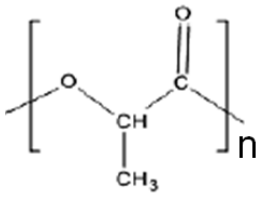

Figure 4.3 The skeletal formula of polylactic acid

Figure 4.4 shows a typical Raman spectrum of untreated MFC reinforced PLA composites. Two features can be seen in this spectrum, (1) relatively higher intensity around 1095 cm^{-1} compared to that of 1122 cm^{-1}, the pattern of which can also be found in the spectrum of MFC (Figure 4.2), but not in that of PLA; (2) a unique high peak at 1773 cm^{-1}, corresponding to the carbonyl group of PLA (Kister *et al.* 1998), as seen in Figure 4.3. The overall spectrum of the composite, however, is very similar to the neat PLA spectrum due to the high fraction of PLA in the composite sample. Therefore, it is intuitive to isolate MFC band from composite spectrum by subtracting a separately obtained neat PLA spectrum from the composite spectrum.

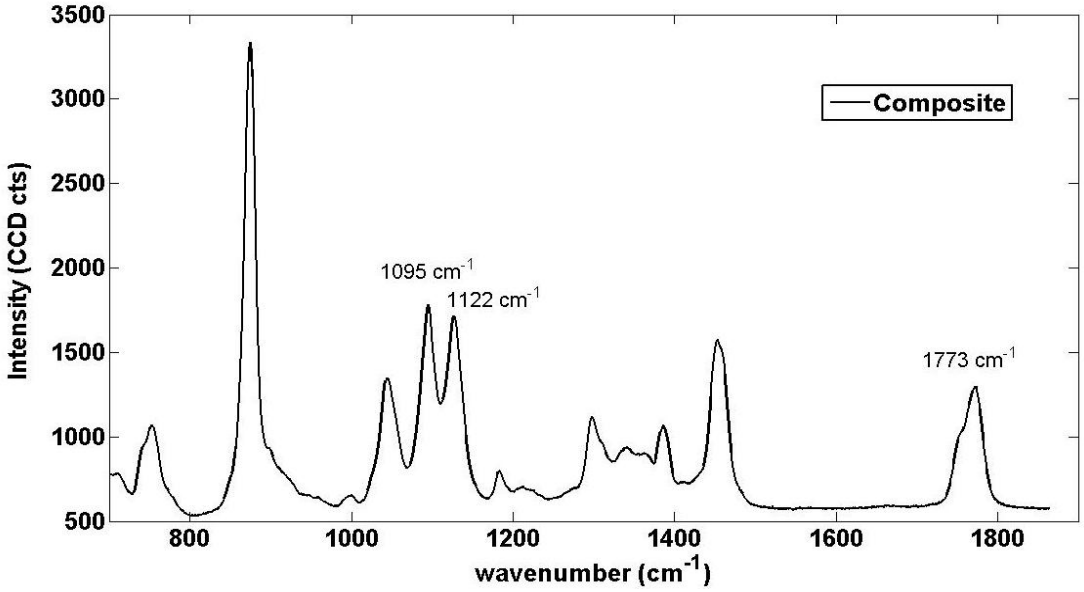

Figure 4.4 Raman spectrum of composite with untreated MFC

An adjusting factor was multiplied with the spectrum of neat PLA in the subtraction to compensate the signal intensity difference between the spectrum of PLA matrix and that of the composite. For example, if the neat PLA signal is higher in intensity, an appropriate value for the factor would be less than one so that the intensity is reduced prior to subtraction.

The adjusting factor was computed using an algorithm adopted from a method by Banerjee and Li (Banerjee and Li 1 July 1991), in which a completely subtracted spectrum (Figure 4.5B) would exhibit a first derivative curve that has a minimum absolute area compared to under- or over-subtraction (Figure 4.5C and 4.5D). Thus, the adjusting factor was optimized to acquire a subtracted spectrum whose first derivative curves had a minimum absolute area (Figure 4.6). This optimization of adjusting factor was to address a scenario where incomplete removal of certain PLA bands, if any, may potentially affect the cellulose band shift analysis. This scenario is critical when certain peaks of the matrix (PLA) in the composite spectra shift slightly due to molecular interactions with the fibers.

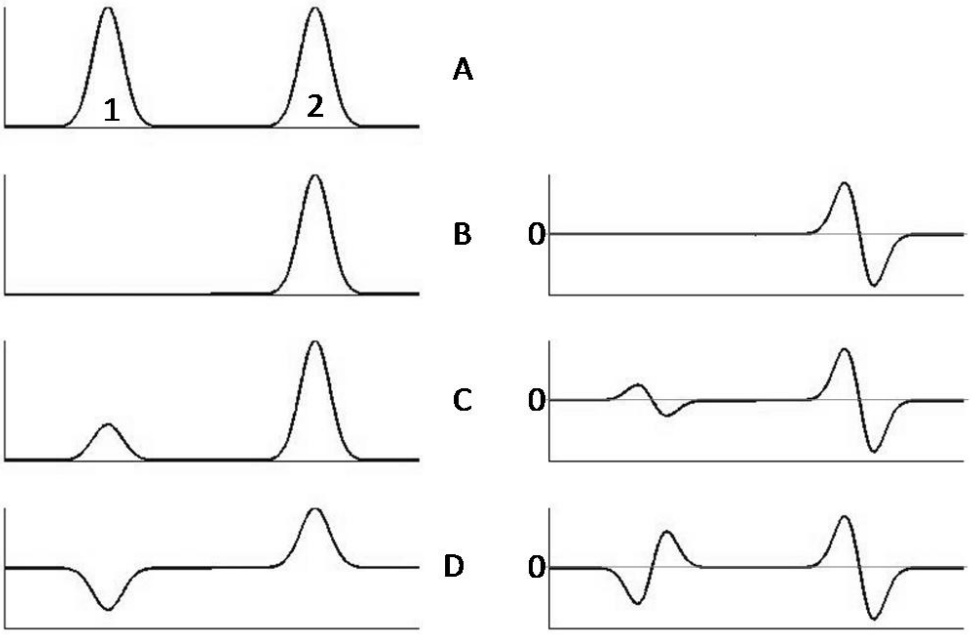

Figure 4.5 A multicomponent spectrum (A) and subtracted spectra (B-D) with their respective first derivatives (right). Component 1 is (B) completely, (C) under-, and (D) over-subtracted.

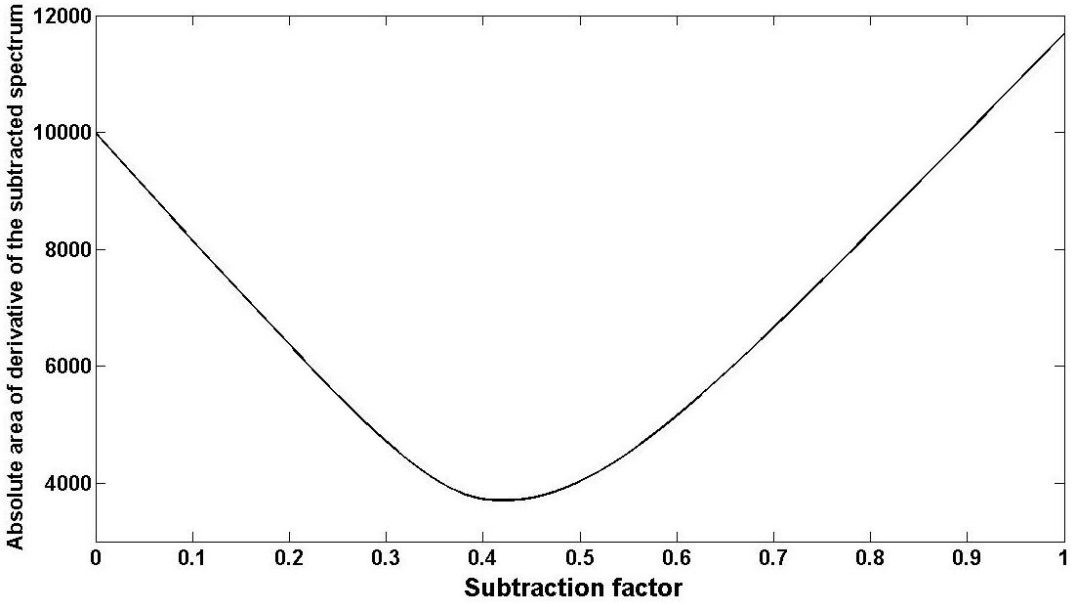

Figure 4.6 Optimization process of acquiring the subtraction adjusting factor

Figure 4.7 shows a spectrum of subtracted composite using an adjusting factor of 0.419 computed from the algorithm mentioned above. The spectrum was favorably similar to that of neat MFC.

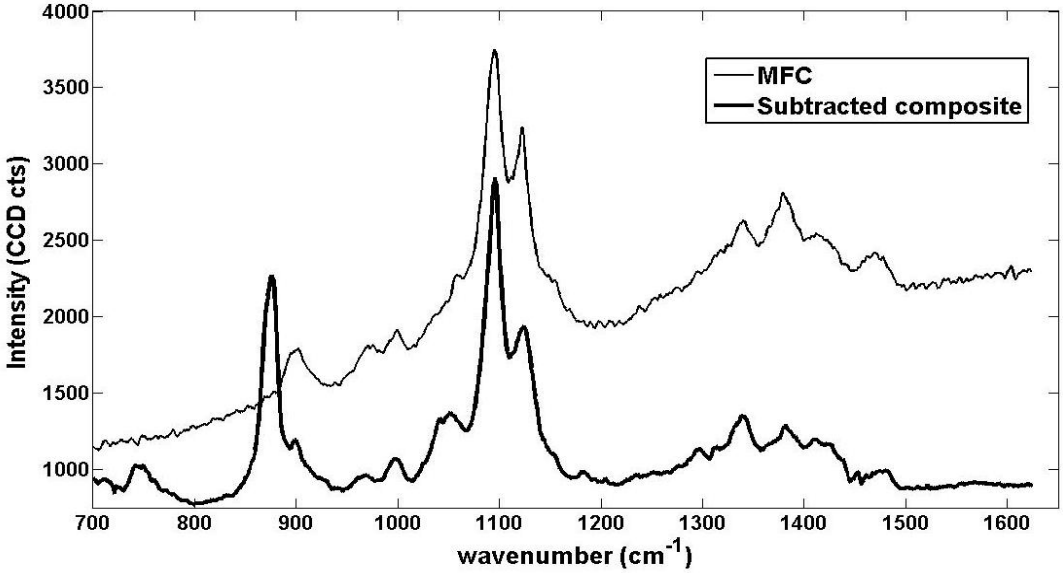

Figure 4.7 Raman spectrum of neat MFC and subtracted composite (with untreated MFC) using an adjusting factor of 0.419

In order to quantify the band position of isolated cellulose peak at 1095 cm^{-1}, a curve fitting procedure was performed on subtracted composite spectra within the frequency range of 1020-1172 cm^{-1}. Four Lorentzian/Gaussian peaks were deconvolved using the shareware XPSPEAK 4.1 (Figure 4.8) to determine the position of 1095 cm^{-1} from cellulose fibers.

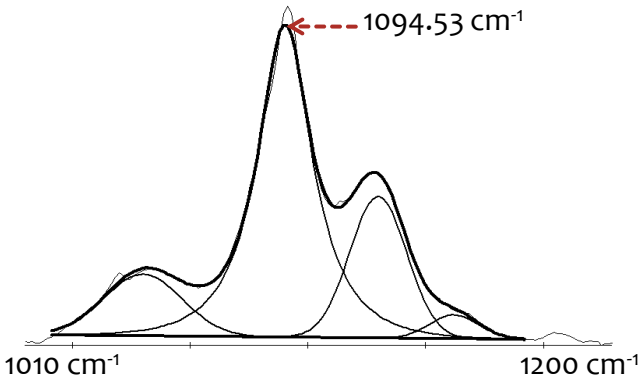

Figure 4.8 Curve-fitting of a composite peak of cellulose to determine the position of the 1095 cm^{-1} peak

4.4.2 Accuracy verification of the test

During each test, it is desirable to maintain the laser focus spot on the same location of the specimen to collect spectra for monitoring local stress changes of the cellulose nano-fibers. However, after each straining of the specimen, the focused laser spot was slightly off the previous location of the specimen due to local deformation along the tensile direction. A refocusing process, therefore, was necessary to ensure the spectrum was acquired on the same location of the composite. The refocusing was performed by first adjusting, along the tensile axis (x axis), the Raman microscope X-Y stage on which the tensile stage was placed. The height of the Raman microscope's objective (z axis) was also readjusted to guarantee the consistency of each spectrum. The target was to find a spectrum pattern similar to that previously obtained, i.e. spectrum intensity and the extent of fluorescence, given that the location previously analyzed (focused with the laser spot) would have no observable fluorescence due to photobleaching. Since the refocusing was manually operated, it is possible that the spectrum may not be taken at the exact same

location, but with certain variability. Hence, it is necessary to verify to what extent the refocusing would affect the accuracy of the test.

Table 4.1 Results of accuracy test, where z-on the height direction, x-on the tensile axis direction, SD---standard deviation, position---relative to the reference point

Axis	Position (μm)	Peak (cm^{-1})	SD(cm^{-1})
Reference	0	1094.76	
Z	1	1094.79	0.0538
	2	1094.84	
	3	1094.85	
	-1	1094.82	
	-2	1094.85	
	-3	1094.93	
X	1	1094.93	0.0926
	2	1094.88	
	-1	1095	
	-2	1094.96	

An individual test was performed to simulate the refocusing process where several spectra were collected from different spatial positions relative to a reference point on an unstrained composite film. The scope of these spots was up to 3 μm along x and z directions of the reference point, which was considered as a reasonable range in the real refocusing process. The spectra obtained were processed according to the protocol described in the previous section. Table 4.1 lists the result and the standard deviation compared to the wavenumber of the reference point. The result indicates that any band shift more than 0.1 cm^{-1} is significantly related to molecular deformation rather than variability resulting from the refocusing process.

4.4.3 Time effect on Raman band shift in composites

A load trend recorded on a composite specimen during the test is plotted in Figure 4.9. The abrupt increase in load corresponds to the time when the specimen was stretched to a certain strain level (up to 1.5% strain with 0.5% per stretch). The relaxation portions of the load trend correspond to the time when the specimen was held at a certain strain level. During the first 5 min after each stretch, a rapid drop in the load level resulting from instantaneous relaxation of the specimen may affect the collected Raman spectrum because a spectrum took 4 min to acquire. After the first 5 min, however, the load on the specimen was relatively stable as observed from comparisons of load changes for 5-min time intervals depicted in Figure 4.9 for 1% strain level. The same conclusion was also derived for the first stretch (0.5% strain level) and the third stretch (1.5% strain level). Therefore, spectra were only collected after 5 min of each stretch when the load level of the composite specimen was relatively steady to ensure the stability of the obtained spectra.

Three spectra were acquired after the first 5 min of each stretch to increase statistical reliability. A typical band shift trend was plotted in Figure 4.10. At each strain level, the variability of band shifts was below 0.1 cm^{-1} of the test accuracy level, suggesting the transferred load on the cellulose fiber remained relatively stable during the spectra collection.

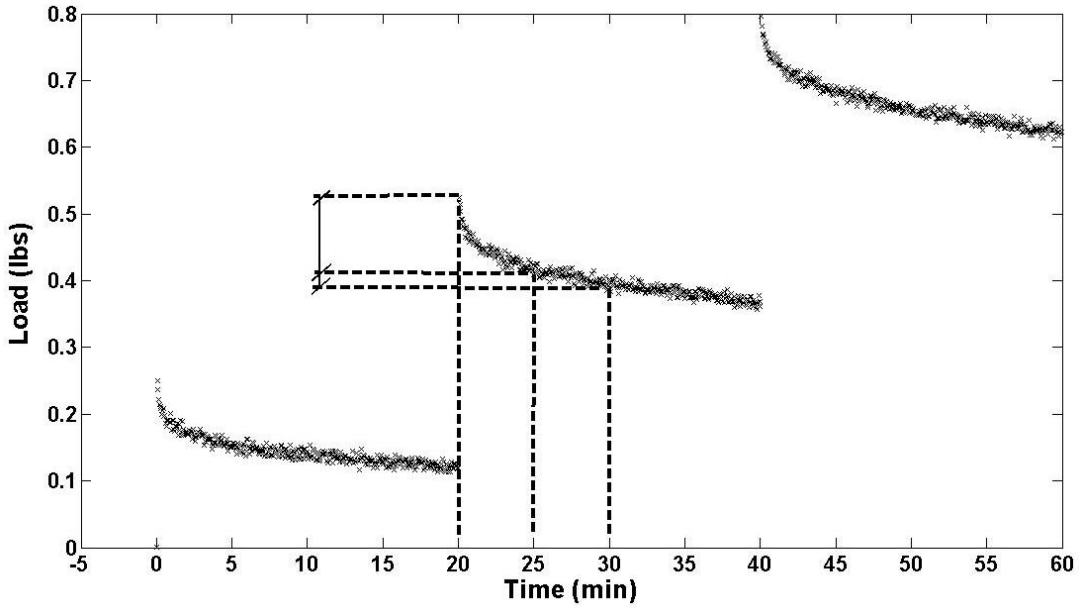

Figure 4.9 Typical load trend during the test on a composite sample with untreated MFC. Load comparison is only marked on the second stretch of the sample.

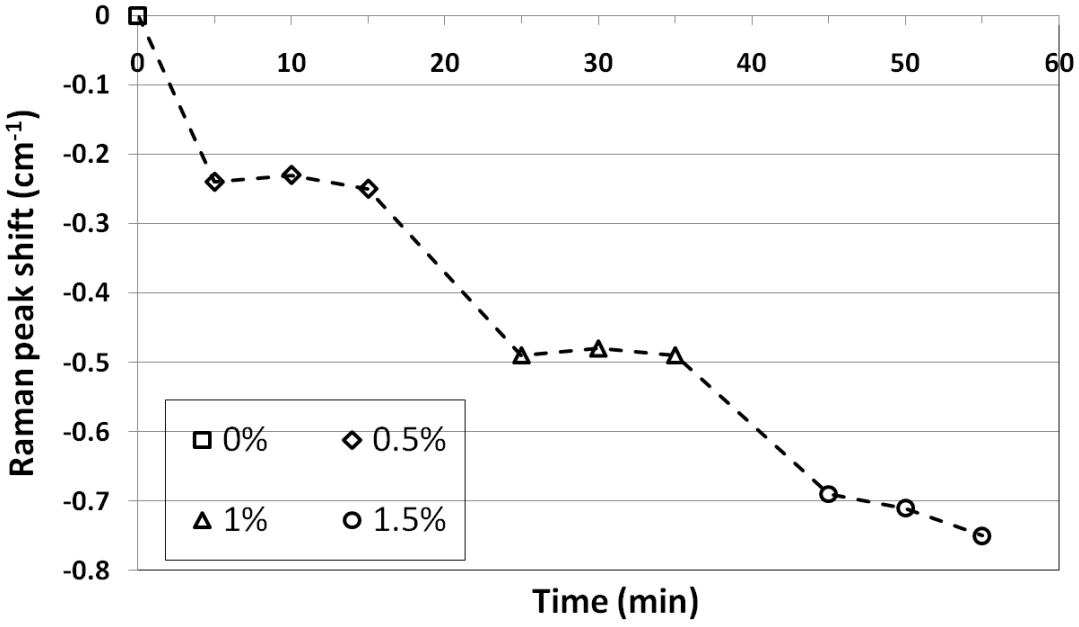

Figure 4.10 Typical band shift trend during the test on a composite sample with treated MFC

4.4.4 Effect of PLA Raman band shift

Although the subtraction step in the spectrum processing protocol minimized the intensity contribution of the PLA signals to the overall composite signals, there is a small peak around the 1095 cm^{-1} in the neat PLA spectrum (Figure 4.2). It is therefore of interest to investigate if this small peak of PLA would also shift with external loading, in which case would adversely interfere with the cellulose band shift analysis. To investigate the possibility of this scenario, a neat PLA sample was strained and examined for Raman bands, as in the case of composite samples.

Figure 4.11a plots the neat PLA Raman band around 1095 cm^{-1} before (0% strain) and after stretching to 1% and 2% strain levels. The small peak from PLA was found not to shift after tensile deformation. For comparisons, the 1095 cm^{-1} band of the composite subjected to tensile loads was also monitored, and the band shift was evident (Figure 4.11b). This conclusion was later validated by comparing the curve fitting results (Table 4.2) from spectra of the neat PLA and composite (after spectra subtraction). The 0.07 cm^{-1} shift for PLA strained at 2% level was considered to not significant enough to affect the cellulose band shift since the value is within the test variability (0.1 cm^{-1}) as already verified in section 0.

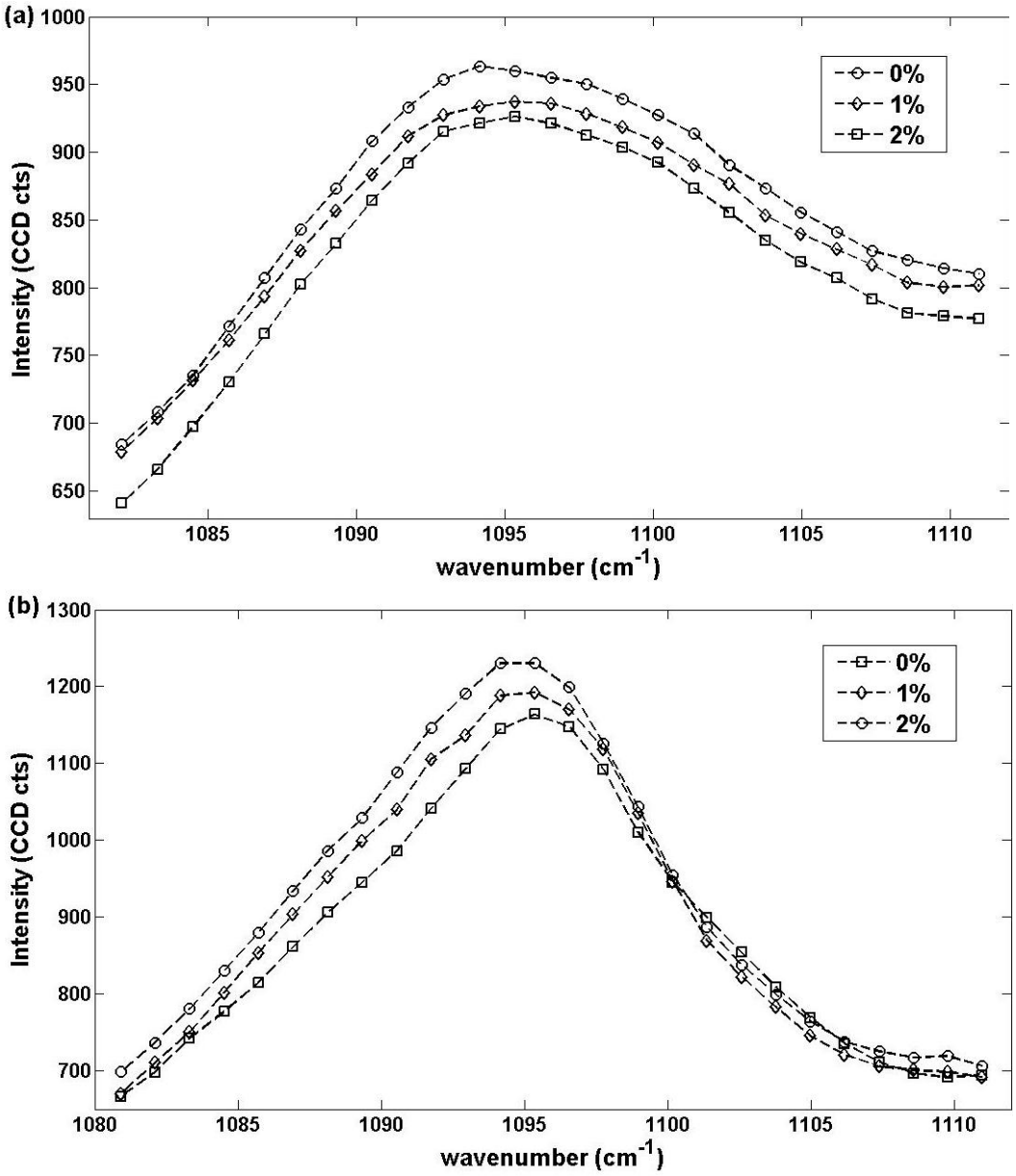

Figure 4.11 Typical Raman spectra for (a) neat poly(lactic acid) (PLA) around 1095 cm^{-1} with different strain levels and (b) composite around the same region at different strain levels (spectra subtracted from a neat PLA spectrum)

Table 4.2 Comparison of Raman band shift at different strain levels between PLA and a composite sample with untreated MFC (shift relative to 0% strain of corresponding sample)

Strain level	PLA Peak shift (cm^{-1})	Composite Peak shift (cm^{-1})*
0%	0	0
1%	0	-0.55
2%	0.07	-0.77

* Composite peak shifts were obtained from the composite spectrum subtracted from neat PLA spectrum using the processing method mentioned in section 4.3.1.

4.5.Conclusion

A spectra processing protocol was established to isolate cellulose spectra from Raman spectra of microfibrillated cellulose/PLA composites and to determine the position of the 1095 cm^{-1} stress-sensitive peak. This protocol was applied to compare Raman band shifts of neat PLA and MFC/PLA samples. It was concluded that the Raman band of PLA around 1095 cm^{-1} did not affect the frequency shift of cellulose nano-fibers with reference to the verified accuracy (standard error < 0.1 cm^{-1}) of this protocol.

4.6. References

Banerjee S, Li D (1991) Interpreting multicomponent infrared spectra by derivative minimization. Applied Spectroscopy 45:1047-1049(3).

Bhardwaj R, Mohanty AK (2007) Modification of brittle polylactide by novel hyperbranched polymer-based nanostructures. Biomacromolecules 8(8):2476-2484.

Eichhorn SJ, Sirichaisit J, Young RJ (2001) Deformation mechanisms in cellulose fibres, paper and wood. Journal of Materials Science 36(13):3129-3135.

Eichhorn SJ, Young RJ, Davies GR (2005) Modeling crystal and molecular deformation in regenerated cellulose fibers. Biomacromolecules 6(1):507-513.

Hamad WY, Eichhorn S (1997) Deformation micromechanics of regenerated cellulose fibers using raman spectroscopy. Journal of Engineering Materials and Technology 119(3):309-313.

Herrick FW, Casebier RL, Hamilton JK, Sandberg KR (1983) Microfibrillated cellulose: Morphology and accessibility. Journal of Applied Polymer Science: Applied Polymer Symposium 37(815):827.

Hwang GL, Shieh Y-, Hwang KC (2004) Efficient load transfer to polymer-grafted multiwalled carbon nanotubes in polymer composites. Advanced Functional Materials 14(5):487-491.

Kister G, Cassanas G, Vert M (1998) Effects of morphology, conformation and configuration on the IR and raman spectra of various poly(lactic acid)s. Polymer 39(2):267-273.

Mitra VK, Risen J,William M., Baughman RH (1977) A laser raman study of the stress dependence of vibrational frequencies of a monocrystalline polydiacetylene. The Journal of Chemical Physics 66(6):2731-2736.

Oksman K, Mathew AP, Bondeson D, Kvien I (2006) Manufacturing process of cellulose whiskers/polylactic acid nanocomposites. Composites Science and Technology 66(15):2776-2784.

Quero F, Nogi M, Yano H, Abdulsalami K, Holmes SM, Sakakini BH, Eichhorn SJ (2009) Optimization of the mechanical performance of bacterial Cellulose/Poly(l-lactic) acid composites. ACS Applied Materials & Interfaces.

Ragauskas AJ, Williams CK, Davison BH, Britovsek G, Cairney J, Eckert CA, Frederick WJ, Jr., et al. (2006) The path forward for biofuels and biomaterials. Science 311(5760):484-489.

Schultz J, Lavielle L, Martin C (1987) The role of the interface in carbon fibre-epoxy composites. The Journal of Adhesion 23(1):45.

Stenstad P, Andresen M, Tanem B, Stenius P (2008) Chemical surface modifications of microfibrillated cellulose. Cellulose 15(1):35-45.

Tripathi D, Jones FR (1998) Single fibre fragmentation test for assessing adhesion in fibre reinforced composites. Journal of Materials Science 33(1):1-16.

Wiley JH, Atalla RH (1987) Band assignments in the raman spectra of celluloses. Carbohydrate Research 160:113-129.

Young RJ, Eichhorn SJ, Shyng Y, Riekel C, Davies RJ (2004) Analysis of stress transfer in two-phase polymer systems using synchrotron microfocus X-ray diffraction. Macromolecules 37(25):9503-9509.

Chapter 5 Effect of microfibrillated cellulose (MFC) chemical modification and loading ratio on the load transfer in MFC/poly(lactic acid) (PLA) composites

5.1.Chapter summary

The load transfer between poly(lactic acid) (PLA) and micrfibrillated cellulose (MFC) was investigated by Raman-tensile tests. MFC was modified with oligomeric lactic acid. The modified MFC was loaded into a PLA solution before being cast into a film. The nanocomposite films were subjected to tensile loading during which Raman spectroscopy was performed under a microscope. The Raman spectrum of MFC was isolated from the spectrum of its composites. The stress-sensitive Raman band of cellulose (1095 cm^{-1}) was analyzed for wavenumber shift, which is an indication of load transfer from the PLA matrix to MFC. Compared to the control (untreated) sample, composites with lactide-treated MFC exhibited a higher Raman band shift as a response to both applied strain and stress, indicating an improved efficiency of load transfer across the compatibilized interphase between nanofibers and PLA. The effect of MFC addition ratio on the load transfer ability was also discussed. A higher MFC weight fraction (0.5 % versus 0.25 %) in the composite did not significantly affect the load transfer efficiency. This finding suggests that the efficiency of matrix/filler load transfer at the local level is independent of the effects of macroscopic filler-to-matrix ratio, at least at the (low) levels of MFC loading examined in this study. Overall, this research shows that it is feasible to use Raman spectroscopy to monitor load transfer in MFC/PLA composites for examining strategies aimed at improving adhesion and knowledge of the mechanism of PLA reinforcement by nano-cellulose.

5.2.Introduction

Poly(lactic acid) (PLA) is one of the promising biopolymers to replace petroleum based plastics not only because of its biodegradability and biocompatibility (Ragauskas *et al.* 2006), but also its possibility to be processed on standard plastic equipment (Nakagaito *et al.* 2009). However, the inherent brittleness of PLA has been a major drawback for its large-scale commercial applications (Bhardwaj and Mohanty 2007). Preparation of biocomposites has become an attractive approach to enhance the mechanical properties of PLA, because of the renewability and biodegradability of both material matrix and reinforcement (Oksman *et al.* 2006).

One candidate for biobased reinforcing agents for PLA is nano-sized cellulose elements from plant cell walls. Linear cellulose chains in plant cell walls aggregate into microfibrils of 2 to 20nm in diameter, and several tens of microns in length (Azizi Samir *et al.* 2005). These microfibrils are embedded in a matrix of hemicelluloses and lignin to provide structural support to the cell wall. If these structural and nano-sized microfibrils can be isolated from plant cell walls and utilized as a reinforcing phase in composites, the performance of the resultant composites can be highly improved.

Microfibrillated cellulose (MFC), first introduced by Turbak et al.(1983), is produced by imposing repeated high-pressure mechanical shearing forces on dilute slurries of cellulose fibers through a "homogenizing" machine (Herrick *et al.* 1983). This shearing action yields a highly entangled network which typically consists of elements (fibrils) having a wide distribution of diameter down to nanoscale (Herrick *et al.* 1983). MFC is thus regarded a nano-cellulose. This nano-cellulose is exceptionally large in specific

surface area (Stenstad *et al.* 2008) and (2) highly accessible by cellulase enzyme (Herrick *et al.* 1983), thereby allowing surface functionalization for improved interactions with bioplastics to favor reinforcement, while maintaining its end-of-life biodegradation advantage.

Despite the high potential of MFC in bioplastic reinforcement, MFC, due to the high density of surface hydroxyl groups, cannot be uniformly dispersed in polymer media that are relatively low in polarity. The cellulose fibrils tend to from hydrogen bonds with adjacent fibrils instead of interacting with the surrounding matrix (Sirόand Plackett 2010). It is, therefore, necessary to modify the surface of MFC so that it can be compatible with less hydrophilic polymers. One of the surface modification methods for polymers in general is to coat oligomer dispersant on MFC. Wang and Sain (2007b) studied the reinforcement effect of ethylene-acrylic oligomer emulsion coated MFC on polyethylene (PE) and polypropylene (PP). Compared to unfilled polymers(PP or PE)/acrylic blends, the composites with 5 wt% oligomer coated nanofibers exhibited significant improvement in modulus (62% and 92% for PE and PP, respectively) and tensile strength (26% and 146% for PE and PP, respectively). This favorable result verified the effective dispersion of MFC in hydrophobic matrixes. By grafting N-Octadecyl isocyanate on MFC, Siqueira *et al*. (2009) evaluated the effect of the grafting agent on the compatibility of MFC with polycaprolactone (PCL) matrix. They observed, compared to the neat PCL matrix, an increase (60%) in the modulus of the composites with only 3 wt% surface-modified MFC, but not in the case of unmodified MFC because of poor dispersibility of the latter.

There have been several published studies about reinforcing PLA with MFC. Iwatake *et al.* (2008) obtained a PLA/MFC composite with 25% higher tensile strength and 40% higher Young's modulus than those of a neat PLA resin sheet, without compromising the yield strain. Chakraborty *et al.* (2005) also compounded PLA with cryocrushed MFC, which were found uniformly dispersed in the polymer matrix, but the mechanical properties of the composites were not reported in their paper. Nakagaito *et al.* (2009) developed a method similar to the papermaking procedures to produce MFC/PLA composites where a good dispersion of MFC was obtained even at high MFC contents. They studied the effect of MFC loading ratio on the mechanical properties of composites and found the modulus and strength of composites were improved as the content of MFC increased from 10 - 70 wt%.

Although MFC reinforcement of PLA was evident as reviewed above, the reinforcement is expected to be further enhanced if appropriate surface modification treatments are performed on MFC. Published studies are limited, however, on the surface modification of MFC for improving mechanical properties of PLA. Of these studies, Wang and Sain (2007a) examined the effect of styrene maleic anhydride treatment of MFC on the reinforcement of PLA resin. From transmission electron microscopy (TEM), cellulose nanofibers extracted from hemp fibers were observed to have partially dispersed in the PLA matrix. It was reported that surface treatments of the reinforcing MFC enhanced the modulus and tensile strength of the neat PLA material by 10% and 8.6% respectively. However, the surface treatment only increased the tensile strength and modulus of the filled PLA composite by 3% and 7%, respectively, compared to composites containing

untreated cellulose nanofibers. This implies that a better surface treatment method needs investigating.

The objective of this chapter was to study the effect of chemical modification and loading level of MFC on the load transfer ability in MFC/PLA composites. Oligomeric lactic acid will be used to modify surfaces of MFC for improved interaction with PLA to ultimately attain polymer reinforcement. To assess if the surface modification improved fiber/matrix interaction, the load transfer efficiency across the MFC/PLA interphase was examined using the Raman-tensile technique following a technical protocol developed in chapter 4.

5.3.Materials and methods

PLA (injection-molding grade 3051D) was purchased from NatureWork LLC. MFC was obtained from the University of Maine research team of the Forest Bioproducts Research Initiative. The MFC was reacted with lactide (Figure 5.1) at 180 ^{o}C for 1 hour. The modified MFC samples (0.25 dry-wt % and 0.5 dry-wt %) were blended into a PLA (6 wt%) solution of dichloroethane before being cast into a film. For comparison, the same amount of untreated MFC was used to form the control sample. All composite films were prepared by the research group of Professor John Simonsen (Oregon State University) with whom we have an ongoing collaborative research.

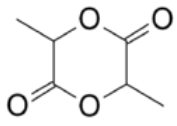

Figure 5.1 The formula of lactide

The composite film was cut into rectangular pieces and glued with a fast-curing epoxy on a home-made mini tensile stage at least 24 hours before each test. The thickness of the samples was 0.03-0.04 mm with width in a range of 2-3 mm. To implement the Raman-tensile test, the tensile stage was placed under a confocal Raman microscope (WITec alpha300R). The specimen was stretched at a speed of 7.5 mm/min with an incremental strain of 0.5% (for 0.5% MFC loading ratio) or 0.25% (for 0.25% MFC loading ratio) of 15-16 mm initial gap between two gripping clamps. After each stretch, the film was held in position for spectra collection. This process was repeated up to a maximum strain value of 1.5% to ensure that the loading was within its linear elastic range of the composite specimen (Figure 5.2).

The linear elastic region of MFC/PLA composite films was determined from two composite samples with treated or untreated MFC using the same tensile stage with a testing speed of 0.6 mm/min. The specimen strip was glued with a fast-curing epoxy resin and mounted for at least 24 hours before each test. Sample width and thickness were determined by using a vernier caliper after the sample fractured.

The confocal Raman microscope equipped with an Ar-ion laser of 514.5 nm was polarized along the strain axis of the tensile stage, unless otherwise stated. After the laser was focused onto a selected area of the composite film using a Nikon 10x objective (0.3 numerical aperture), a spectrum was obtained in a backscattering geometry with a laser power of 35 mW in 4 min. A 10x, as opposed to objective lens with higher magnification, was used to reduce spatial errors from the refocusing process due to local deformation when the composite was stretched. Raman spectrum was processed using a protocol

discussed in chapter 4. The Raman band shift was plotted with corresponding strain or stress recorded by a 50lb load cell with an accuracy of 0.7% full scale.

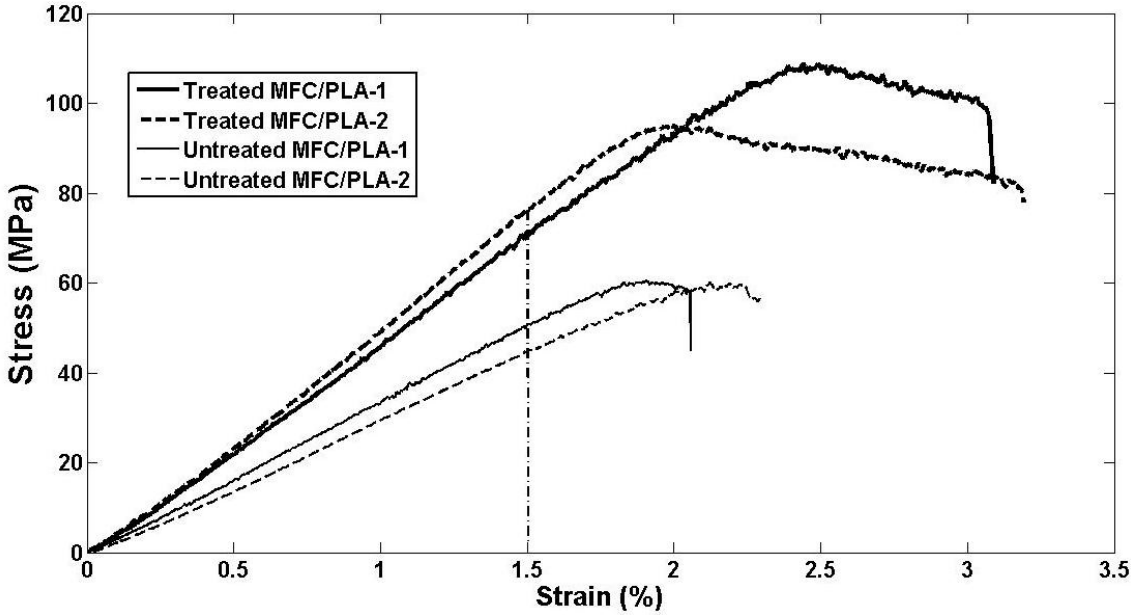

Figure 5.2 Stress-strain curves for composite with 0.25% untreated MFC (two samples) and composite with 0.25% treated MFC (two samples).

5.4.Results and discussion

5.4.1 Effect of MFC orientation

In the PLA matrix, the MFC was randomly oriented. At the local level, however, the Raman band shift was monitored from an embedded MFC of specific orientation. The inferred load transfer ability, therefore, corresponds specifically to that MFC orientation. It has been recognized in general that a reinforcing fiber aligned parallel to the loading axis of the composite would allow the largest load transfer compared to off-axis orientation. In order to examine the effect of MFC orientation, Raman-tensile tests were individually performed on MFC elements oriented at different angles relative to the

tensile axis of the composites. Figure 5.3 plots the 1095 cm^{-1} band shift rate of MFC at different orientation, with zero degree being parallel to the tensile axis of the composite. The angle values were measured from microscopic pictures of composite samples using the ImageJ shareware (Figure 5.4). It is noteworthy that under such magnification (10x objective lens), only the MFC main element was visible but not the branched fibrils. The band shift rate (cm^{-1}/% strain) was determined from the slope of a linear plot of band shift (cm^{-1}) versus applied strain level (in %). For MFC with an alignment angle greater than 50 degrees, the band shift rate was obtained from the peak shift when the composite was stretched to 1% strain.

The band shift becomes positive at an MFC alignment angle greater than about 60 degrees (Figure 5.3), indicating that the 1095 cm^{-1} band of cellulose shifted to a higher wavenumber when a strain was applied on the composite. This positive shift is a manifestation of compression exerted onto the longitudinal axis of the MFC due to the Poisson contraction of the composite as it is strained. The dependence of Raman band shift rate on the fiber alignment angle θ can be expressed as (Cooper *et al.* 2001),

$$e_\theta = e_0(cos^2\theta - \frac{1}{3}sin^2\theta)$$

where e_0 is the band shift rate of MFC parallel to the tensile axis of the composite, and ⅓ is the approximate Poisson ratio of the composite. The dashed curve on Figure 5.3 was plotted using the equation above. The experiment data approximated the fitted values.

Since the MFC orientation would affect the band shift rate of cellulose at 1095 cm^{-1}, subsequent discussions will be focused on MFC parallel to the tensile axis of the composite for examination of load transfer ability.

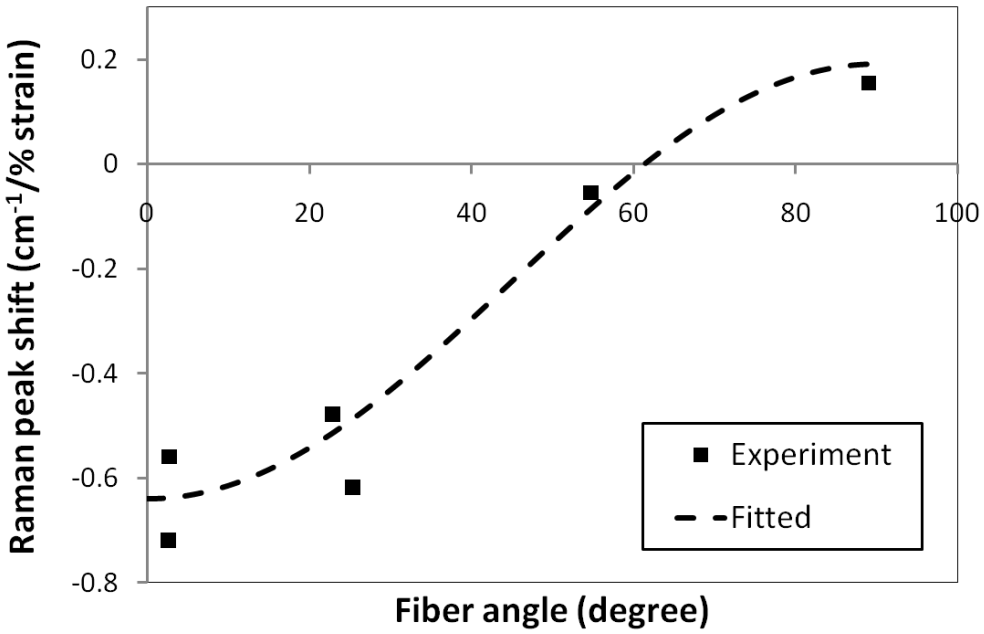

Figure 5.3 Dependence of the peak shift of the 1095cm^{-1} Raman band on fiber angle oriented at angle to the tensile axis.

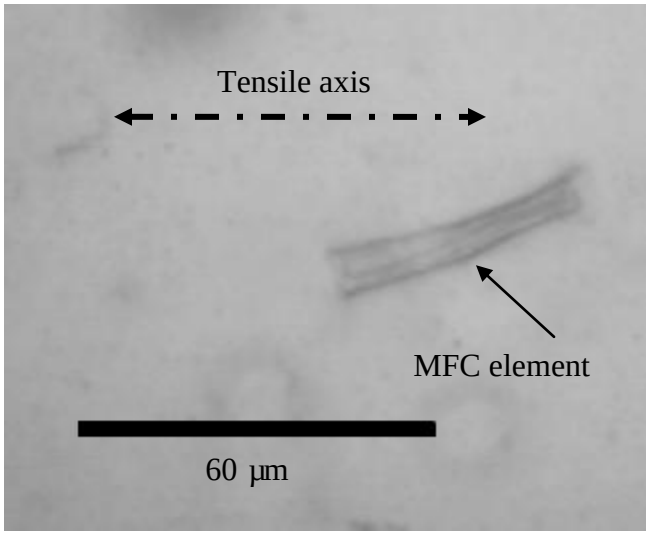

Figure 5.4 A typical microfibrillated cellulose fiber embedded in PLA matrix

5.4.2 Effect of MFC treatment and loading ratio on load transfer

When the MFC/PLA composites were under tension, the Raman band of cellulose peak at 1095 cm^{-1} shifted towards lower wavenumber as discussed in chapter 4. The shift of this cellulose peak was linearly dependent on the strain applied to the composites up to a level of about 1.5% (Figure 5.5a). The shift rate with respect to applied strain levels was determined from the slope of a linear line fitted to experimental data. A value of -0.91 cm^{-1}/% strain was obtained for a typical composite sample (0.25 wt% MFC) with lactide-treated MFC, which was higher than 0.78 cm^{-1}/% strain for a typical control specimen. Since the amount of band shift (cm^{-1}) relates to the magnitude of tensile stress in the cellulose fiber, it can be concluded that at an applied strain level (e.g. 1% on composite), a higher load was transferred to lactide-treated MFC than untreated MFC in the respective composites.

The effect of load transfer can be better appreciated by plotting the peak shift of cellulose at 1095 cm^{-1} with respect to the stress exerted to composites (Figure 5.5b). A much greater band shift per unit applied stress was attained for the MFC/PLA composites with surface treatment (-0.026 cm^{-1}/MPa) than for composite with no treatment (-0.016 cm^{-1}/MPa). This result indicates that a portion of load applied on composites was transferred to MFC, leading to stressing or straining of the molecular backbone of cellulose. The higher band shift rate of lactide-treated MFC signifies a higher load transfer to the MFC fiber when fiber/matrix compatibility was improved. It is interesting to point out there was small deviation from the fitted linear line when composite samples were stretched to 1.5% strain level (as indicated by dotted square in Figure 5.4). One of possible reasons for this

deviation was that 1.5% strain was beyond the linear elastic region of MFC in composites, where stress on the MFC no longer linearly responded to strain of MFC in composite films.

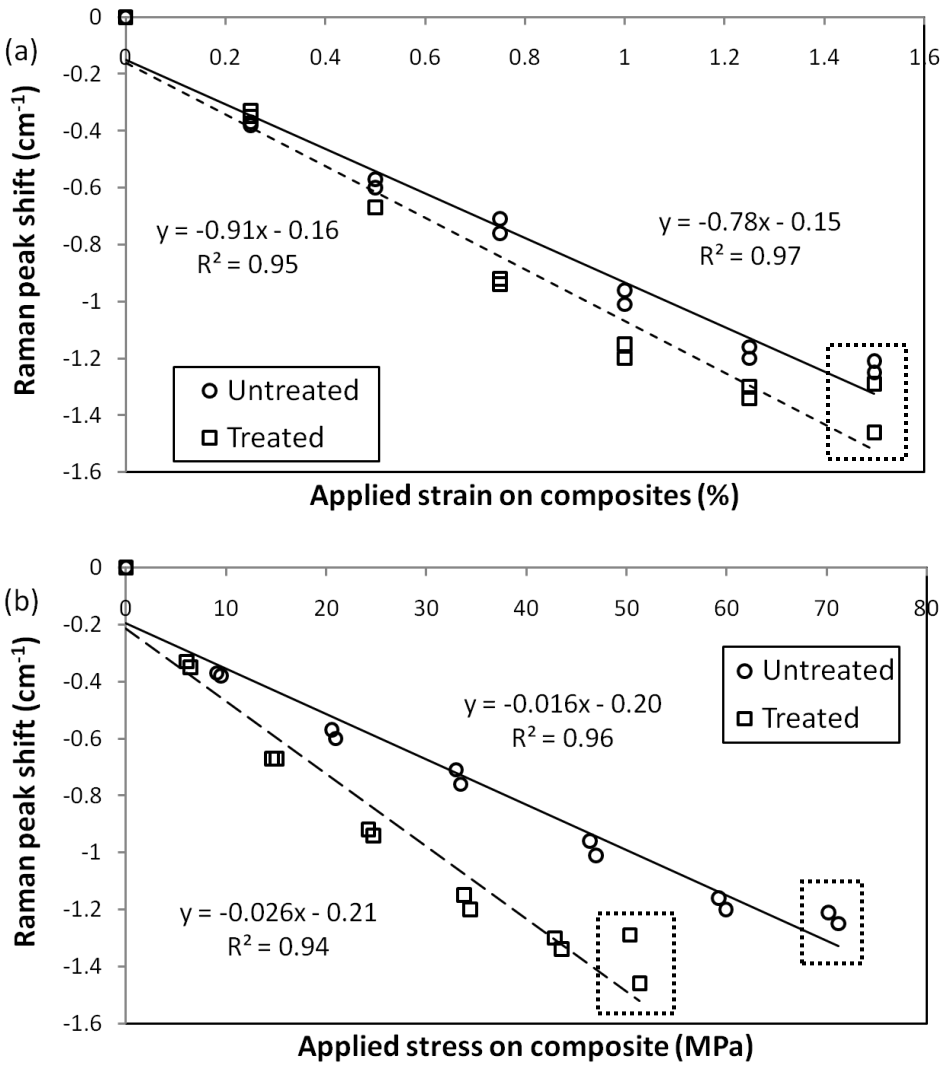

Figure 5.5 Typical (a) Raman peak shifts of 1095 cm^{-1} for 0.25 wt% lactide treated and untreated MFC/PLA composite with respect to strain on the sample, (b) Raman peak shifts of 1095cm^{-1} for lactide treated and untreated MFC/PLA composite with respect to applied stress on the composite

Figure 5.6 compares the band shift rates between untreated and treated MFC and also between lower and higher MFC loading levels (0.25 versus 0.5 wt%). Composites with

0.5 wt% MFC also exhibit an increased load transfer with MFC surface treatments, similar to the case of lower MFC loading (0.25 wt%) discussed earlier. For a given MFC (untreated or treated), the Raman peak shift for every 1% strain appeared to be higher in 0.25 wt% than 0.5 wt% loading (Figure 5.6a). This observation can be explained by the apparent modulus calculated from the load exerted to the composites when they were strained at 1%. As seen in Figure 5.7, most of 0.25 wt%-MFC/PLA composites exhibited higher apparent moduli than composites with 0.5 wt% MFC, and the difference could be attributed to the temperature ("softening" effects) at which the Raman-tensile tests were performed. Since in general composites with 0.25 wt% MFC had higher apparent moduli, a higher stress would be exerted to the composites at a given level of strain. It follows that a higher load was transferred to the MFC fiber compared to the case of 0.5 wt% MFC loading. Thus the higher peak shift rate here should not be interpreted as a higher load transfer ability in composites of 0.25 wt% than 0.5 wt% MFC.

When comparing at the basis of composite stress, the rates of Raman peak shift (cm^{-1}/MPa) were insignificantly different for two MFC loading levels (Figure 5.6b). This observation supports the explanation presented earlier for the band shift rate per percent strain (cm^{-1}/% strain). Indeed, the fiber loading level is a macroscopic parameter, which does not influence the efficiency of load transfer at the local level, especially at such a low loading level ($\leq$0.5 wt%). The only difference derived from the comparisons in Figure 5.6b was between composites of untreated and treated MFC. This difference is a direct manifestation of the higher load transfer ability at compatibilized interphase.

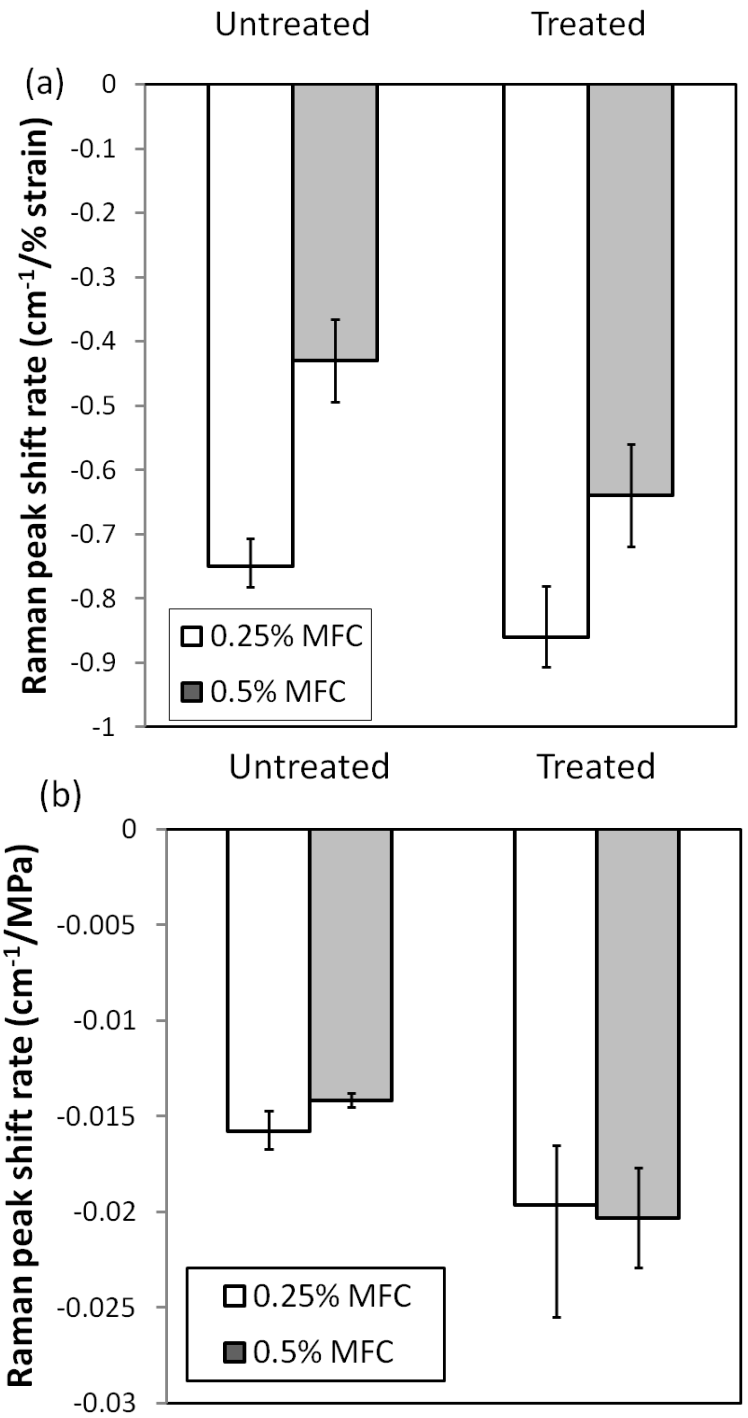

Figure 5.6 Comparison of average Raman band shift of 1095 cm^{-1} cellulose peak for MFC/PLA composites with lactide treated and untreated MFC based on one unit of (a) applied strain, or (b) applied stress on composites of 0.25 wt% and 0.5 wt% MFC loading levels.

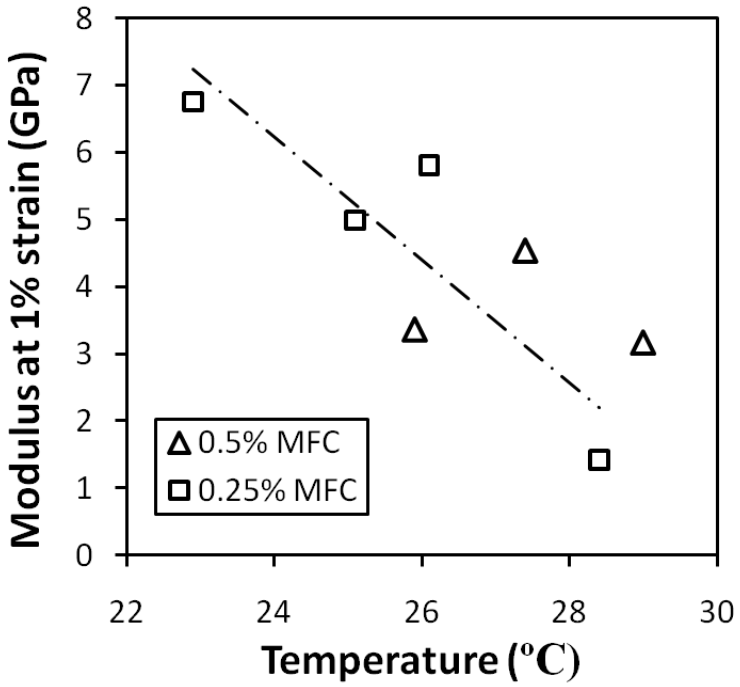

Figure 5.7 Correlation between testing temperatures with apparent modulus at 1% strain of 0.25 wt%- (□) and 0.5 wt% (Δ)-MFC/PLA composites

5.5.Conclusion

This chapter has shown that Raman spectroscopy is a very useful tool to monitor the load transfer mechanism in MFC reinforced PLA bio-composite materials. The load transfer study was accomplished by following the Raman band shift of cellulose at 1095 cm^{-1} with respect to the strain or stress applied to the composite. The transfer of load from PLA matrix to MFC fibers was discussed in the context of surface treatment and loading ratio of MFC. Compared to the control (untreated) sample, composites with treated MFC exhibited higher Raman band shift rates with respect to both applied stress and strain, indicating a better load transfer across the interphase between treated MFC and the polymer matrix (PLA) as a result of compatibilization (lactide treatment of MFC). Loading of MFC at a higher level (0.5 wt% versus 0.25 wt%) did not significantly affect

the load transfer efficiency. This finding suggests that the efficiency of matrix/fiber load transfer at the local level is independent from the effects of macroscopic fiber-to-matrix ratio, at least at the (low) levels of MFC loading examined in this study.

5.6. References

Azizi Samir MAS, Alloin F, Dufresne A (2005) Review of recent research into cellulosic whiskers, their properties and their application in nanocomposite field. Biomacromolecules 6(2):612-626.

Bhardwaj R, Mohanty AK (2007) Modification of brittle polylactide by novel hyperbranched polymer-based nanostructures. Biomacromolecules 8(8):2476-2484.

Chakraborty A, Sain M, Kortschot M (2005) Cellulose microfibrils: A novel method of preparation using high shear refining and cryocrushing. Holzforschung 59(1):102-107.

Cooper CA, Young RJ, Halsall M (2001) Investigation into the deformation of carbon nanotubes and their composites through the use of raman spectroscopy. Composites Part A: Applied Science and Manufacturing 32(3-4):401-411.

Goussé C, Chanzy H, Cerrada ML, Fleury E (2004) Surface silylation of cellulose microfibrils: Preparation and rheological properties. Polymer 45(5):1569-1575.

Herrick FW, Casebier RL, Hamilton JK, Sandberg KR (1983) Microfibrillated cellulose: Morphology and accessibility. Journal of Applied Polymer Science: Applied Polymer Symposium 37(815):827.

Iwatake A, Nogi M, Yano H (2008) Cellulose nanofiber-reinforced polylactic acid. Composites Science and Technology 68(9):2103-2106.

Lönnberg H, Fogelström L, Berglund L, Malmström E, Hult A (2008) Surface grafting of microfibrillated cellulose with poly(ε-caprolactone) – synthesis and characterization. European Polymer Journal 44(9):2991-2997.

Nakagaito AN, Fujimura A, Sakai T, Hama Y, Yano H (2009) Production of microfibrillated cellulose (MFC)-reinforced polylactic acid (PLA) nanocomposites

from sheets obtained by a papermaking-like process. Composites Science and Technology 69(7-8):1293-1297.

Oksman K, Mathew AP, Bondeson D, Kvien I (2006) Manufacturing process of cellulose whiskers/polylactic acid nanocomposites. Composites Science and Technology 66(15):2776-2784.

Ragauskas AJ, Williams CK, Davison BH, Britovsek G, Cairney J, Eckert CA, Frederick WJ, Jr., et al. (2006) The path forward for biofuels and biomaterials. Science 311(5760):484-489.

Siqueira G, Bras J, Dufresne A (2009) Cellulose whiskers versus microfibrils: Influence of the nature of the nanoparticle and its surface functionalization on the thermal and mechanical properties of nanocomposites. Biomacromolecules 10(2):425-432.

Sirόl I, Plackett D (2010) Microfibrillated cellulose and new nanocomposite materials: A review. Cellulose 17(3):459-494.

Stenstad P, Andresen M, Tanem B, Stenius P (2008) Chemical surface modifications of microfibrillated cellulose. Cellulose 15(1):35-45.

Turbak AF, Snyder FW, Sandberg KR (1983) Microfibrillated cellulose, a new cellulose product: Properties, uses, and commercial potential. Journal of Applied Polymer Science: Applied Polymer Symposium 37:815-827.

Wang B, Sain M (2007a) The effect of chemically coated nanofiber reinforcement on biopolymer based nanocomposites. *BioResources* 2(3):371-388.

Wang B, Sain M (2007b) Isolation of nanofibers from soybean source and their reinforcing capability on synthetic polymers. Composites Science and Technology 67(11-12):2521-2527.

Chapter 6 Conclusions and recommendations

In this study, Raman spectroscopy has been demonstrated a powerful tool to examine load transfer at the interphase of microfibrillated cellulose (MFC) reinforced poly(lactic acid) (PLA) composites. A Raman spectrum acquisition and processing protocol was developed to isolate cellulose bands from spectra of composite samples. The accuracy of this protocol was verified on composite films without an applied load. The possible shift of the PLA band around the 1095 cm^{-1} cellulose band of interest was also examined as a function of the applied strain. Based on the accuracy, it is judged that the Raman band of PLA does not interfere with the band shift analysis of cellulose at 1095cm^{-1} as the composite is progressively stretched. This protocol was then applied to study the effect of MFC chemical modification on the load transfer efficiency of MFC/PLA composites. The lactide treated MFC was shown to improve the load transfer efficiency from PLA matrix to MFC fibers, as indicated by the higher Raman band shift rate at a given level of strain or stress applied (or exerted) on the composite. At the levels of MFC loading (0.25 and 0.5 wt%) examined in this study, increasing the fiber weight fraction in the composite did not influence the efficiency of load transfer at the local level.

The usefulness of Raman spectroscopy for studying the load transfer ability of MFC filled PLA composites has been verified. In the future, this technique can be used to map the stress profile of fibers in the composites to investigate the load transfer mechanism and further quantify different interphases created by various modification treatments of either the matrix polymer or reinforcing fibers. The transfer of load at higher MFC weight fractions should also be investigated. Mathematical models should be developed

to describe interfacial adhesion between PLA matrix and MFC reinforcing fibers based on experiment results obtained from different interphases and composition profiles. Through these studies, it is hoped that an optimized interphase could be obtained for enhancing mechanical and other properties of PLA to strategically replace petroleum based plastics.

Bibliography

Ajayan PM, Schadler LS, Braun PV. (2003) Nanocomposite science and technology Weinheim : [Great Britain] : Wiley-VCH, .

Anderson KS, Schreck KM, Hillmyer MA (2008) Toughening polylactide. Polymer Reviews 48(1):85.

Andrews MC, Young RJ (1993) Analysis of the deformation of aramid fibres and composites using raman spectroscopy. Journal of Raman Spectroscopy 24(8):539-544.

Azizi Samir MAS, Alloin F, Dufresne A (2005) Review of recent research into cellulosic whiskers, their properties and their application in nanocomposite field. Biomacromolecules 6(2):612-626.

Banerjee S, Li D (1991) Interpreting multicomponent infrared spectra by derivative minimization. Applied Spectroscopy 45:1047-1049(3).

Barber AH, Cohen SR, Eitan A, Schadler LS, Wagner HD (2006) Fracture transitions at a carbon-Nanotube/Polymer interface. Advanced Materials 18(1):83-87.

Barber AH, Cohen SR, Kenig S, Wagner HD (2004) Interfacial fracture energy measurements for multi-walled carbon nanotubes pulled from a polymer matrix. Composites Science and Technology 64(15):2283-2289.

Barber AH, Cohen SR, Wagner HD (2003) Measurement of carbon nanotube--polymer interfacial strength. Applied Physics Letters 82(23):4140-4142.

Bhardwaj R, Mohanty AK (2007) Modification of brittle polylactide by novel hyperbranched polymer-based nanostructures. Biomacromolecules 8(8):2476-2484.

Boogh LCN, Meier RJ, Kausch H, Kip BJ (1992) A raman microscopy study of stress transfer in high-performance epoxy composites reinforced with polyethylene fibers. Journal of Polymer Science Part B: Polymer Physics 30(4):325-333.

Bruce DM, Hobson RN, Farrent JW, Hepworth DG (2005) High-performance composites from low-cost plant primary cell walls. Composites Part A: Applied Science and Manufacturing 36(11):1486-1493.

Chakraborty A, Sain M, Kortschot M (2005) Cellulose microfibrils: A novel method of preparation using high shear refining and cryocrushing. Holzforschung 59(1):102-107.

Cheng T-, Jones FR, Wang D (1993) Effect of fibre conditioning on the interfacial shear strength of glass-fibre composites. Composites Science and Technology 48(1-4):89-96.

Cooper CA, Young RJ, Halsall M (2001) Investigation into the deformation of carbon nanotubes and their composites through the use of raman spectroscopy. Composites Part A: Applied Science and Manufacturing 32(3-4):401-411.

Cooper CA, Cohen SR, Barber AH, Wagner HD (2002) Detachment of nanotubes from a polymer matrix. Applied Physics Letters 81(20):3873-3875.

Davies RJ, Montes-MorÃ n MA, Riekel C, Young RJ (2001) Single fibre deformation studies of poly(p-phenylene benzobisoxazole) fibres part I determination of crystal modulus. Journal of Materials Science 36(13):3079-3087.

Day RJ, Robinson IM, Zakikhani M, Young RJ (1987) Raman spectroscopy of stressed high modulus poly(p-phenylene benzobisthiazole) fibres. Polymer 28(11):1833-1840.

Drzal LT, Madhukar M (1993) Fibre-matrix adhesion and its relationship to composite mechanical properties. Journal of Materials Science 28(3):569-610.

Dufresne A, Cavaillé J, Vignon MR (1997) Mechanical behavior of sheets prepared from sugar beet cellulose microfibrils. Journal of Applied Polymer Science 64(6):1185-1194.

Dufresne A, Dupeyre D, Vignon MR (2000) Cellulose microfibrils from potato tuber cells: Processing and characterization of starch-cellulose microfibril composites. Journal of Applied Polymer Science 76(14):2080-2092.

Edwards HGM, Farwell DW, Webster D (1997) FT raman microscopy of untreated natural plant fibres. Spectrochimica Acta Part A: Molecular and Biomolecular Spectroscopy 53(13):2383-2392.

Eichhorn SJ, Bennett JA, Shyng YT, Young RJ, Davies RJ (2006) Analysis of interfacial micromechanics in microdroplet model composites using synchrotron microfocus X-ray diffraction. Composites Science and Technology 66(13):2197-2205.

Eichhorn SJ, Sirichaisit J, Young RJ (2001a) Deformation mechanisms in cellulose fibres, paper and wood. Journal of Materials Science 36(13):3129-3135.

Eichhorn SJ, Young RJ, Yeh W- (2001b) Deformation processes in regenerated cellulose fibers. Textile Research Journal 71(2):121-129.

Eichhorn SJ, Young RJ, Davies GR (2005) Modeling crystal and molecular deformation in regenerated cellulose fibers. Biomacromolecules 6(1):507-513.

Eitan A, Fisher FT, Andrews R, Brinson LC, Schadler LS (2006) Reinforcement mechanisms in MWCNT-filled polycarbonate. Composites Science and Technology 66(9):1162-1173.

Frogley MD, Ravich D, Wagner HD (2003) Mechanical properties of carbon nanoparticle-reinforced elastomers. Composites Science and Technology 63(11):1647-1654.

Ganesan Y, Lou J (2009) The mechanical characterization of carbon-nanotube-reinforced polymer-matrix nanocomposites: An unfolding story of interface. JOM Journal of the Minerals, Metals and Materials Society 61(1):32-37.

Gardner DJ, Oporto GS, Mills R, Azizi Samir M,Ahmed Said (2008) Adhesion and surface issues in cellulose and nanocellulose. Journal of Adhesion Science and Technology 22:545-567.

Garlotta D (2001) A literature review of poly(lactic acid). Journal of Polymers and the Environment 9(2):63-84.

Gierlinger N, Schwanninger M, Reinecke A, Burgert I (2006) Molecular changes during tensile deformation of single wood fibers followed by raman microscopy. Biomacromolecules 7(7):2077-2081.

Gousséc, Chanzy H, Cerrada ML, Fleury E (2004) Surface silylation of cellulose microfibrils: Preparation and rheological properties. Polymer 45(5):1569-1575.

Grijpma DW, Altpeter H, Bevis MJ, Feijen J (2002) Improvement of the mechanical properties of poly(D,L-lactide) by orientation. Polymer International 51(10):845-851.

Habibi Y, Mahrouz M, Vignon MR (2009) Microfibrillated cellulose from the peel of prickly pear fruits. Food Chemistry 115(2):423-429.

Hamad WY, Eichhorn S (1997) Deformation micromechanics of regenerated cellulose fibers using raman spectroscopy. Journal of Engineering Materials and Technology 119(3):309-313.

Herrera-Franco PJ, Drzal LT (1992) Comparison of methods for the measurement of fibre/matrix adhesion in composites. Composites 23(1):2-27.

Herrick FW, Casebier RL, Hamilton JK, Sandberg KR (1983) Microfibrillated cellulose: Morphology and accessibility. Journal of Applied Polymer Science: Applied Polymer Symposium 37(815):827.

Hoecker F, Karger-Kocsis J (1996) Surface energetics of carbon fibers and its effects on the mechanical performance of CF/EP composites. Journal of Applied Polymer Science 59(1):139-153.

Hwang GL, Shieh Y-, Hwang KC (2004) Efficient load transfer to polymer-grafted multiwalled carbon nanotubes in polymer composites. Advanced Functional Materials 14(5):487-491.

Iwatake A, Nogi M, Yano H (2008) Cellulose nanofiber-reinforced polylactic acid. Composites Science and Technology 68(9):2103-2106.

Kelly A, Tyson WR (1965) Tensile properties of fibre-reinforced metals: Copper/tungsten and copper/molybdenum. Journal of the Mechanics and Physics of Solids 13(6):329-338, in1-in2, 339-350.

Kim JK. (1998) Engineered interfaces in fiber reinforced composites Elsevier Science Ltd, Burlington.

Kim J-, Zhou L, Mai Y- (1993) Stress transfer in the fibre fragmentation test: Part I an improved analysis based on a shear strength criterion. Journal of Materials Science 28(22):6233-6245.

Kister G, Cassanas G, Vert M (1998) Effects of morphology, conformation and configuration on the IR and raman spectra of various poly(lactic acid)s. Polymer 39(2):267-273.

Leeuw TK, Tsyboulski DA, Nikolaev PN, Bachilo SM, Arepalli S, Weisman RB (2008) Strain measurements on individual single-walled carbon nanotubes in a polymer host: Structure-dependent spectral shifts and load transfer. Nano Letters 8(3):826-831.

Liu L, Barber AH, Nuriel S, Wagner HD (2005) Mechanical properties of functionalized single-walled carbon-Nanotube/Poly(vinyl alcohol) nanocomposites. Advanced Functional Materials 15(6):975-980.

Liu T, Tong Y, Zhang W (2007) Preparation and characterization of carbon nanotube/polyetherimide nanocomposite films. Composites Science and Technology 67(3-4):406-412.

Lönnberg H, Fogelström L, Berglund L, Malmström E, Hult A (2008) Surface grafting of microfibrillated cellulose with poly(ε-caprolactone) – synthesis and characterization. European Polymer Journal 44(9):2991-2997.

Lu J, Askeland P, Drzal LT (2008) Surface modification of microfibrillated cellulose for epoxy composite applications. Polymer 49(5):1285-1296.

Miller B, Gaur U, Hirt DE (1991) Measurement and mechanical aspects of the microbond pull-out technique for obtaining fiber/resin interfacial shear strength. Composites Science and Technology 42(1-3):207-219.

Mitra VK, Risen J,William M., Baughman RH (1977) A laser raman study of the stress dependence of vibrational frequencies of a monocrystalline polydiacetylene. The Journal of Chemical Physics 66(6):2731-2736.

Mu, Minfang, Sebastian Osswald, Yury Gogotsi, and Karen I. Winey. 2009. An in situ raman spectroscopy study of stress transfer between carbon nanotubes and polymer. Abstract. *Nanotechnology* 20, no. 33:335703.

Nakagaito AN, Yano H (2005) Novel high-strength biocomposites based on microfibrillated cellulose having nano-order-unit web-like network structure. Applied Physics A: Materials Science & Processing 80(1):155-159.

———. (2004) The effect of morphological changes from pulp fiber towards nano-scale fibrillated cellulose on the mechanical properties of high-strength plant fiber based composites. Applied Physics A: Materials Science & Processing 78(4):547-552.

Nakagaito AN, Fujimura A, Sakai T, Hama Y, Yano H (2009) Production of microfibrillated cellulose (MFC)-reinforced polylactic acid (PLA) nanocomposites from sheets obtained by a papermaking-like process. Composites Science and Technology 69(7-8):1293-1297.

Oksman K, Mathew AP, Bondeson D, Kvien I (2006) Manufacturing process of cellulose whiskers/polylactic acid nanocomposites. Composites Science and Technology 66(15):2776-2784.

Pääkkö M, Ankerfors M, Kosonen H, Nykänen A, Ahola S, Österberg M, Ruokolainen J, et al. (2007) Enzymatic hydrolysis combined with mechanical shearing and high-pressure homogenization for nanoscale cellulose fibrils and strong gels. Biomacromolecules 8(6):1934-1941.

Paipetis A, Galiotis C (1996) Effect of fibre sizing on the stress transfer efficiency in carbon/epoxy model composites. Composites Part A: Applied Science and Manufacturing 27(9):755-767.

Qian D, Dickey EC, Andrews R, Rantell T (2000) Load transfer and deformation mechanisms in carbon nanotube-polystyrene composites. Applied Physics Letters 76(20):2868-2870.

Quero F, Nogi M, Yano H, Abdulsalami K, Holmes SM, Sakakini BH, Eichhorn SJ (2009) Optimization of the mechanical performance of bacterial Cellulose/Poly(l-lactic) acid composites. ACS Applied Materials & Interfaces.

Ragauskas AJ, Williams CK, Davison BH, Britovsek G, Cairney J, Eckert CA, Frederick WJ, Jr., et al. (2006) The path forward for biofuels and biomaterials. Science 311(5760):484-489.

Robinson IM, Zakikhani M, Day RJ, Young RJ, Galiotis C (1987) Strain dependence of the raman frequencies for different types of carbon fibres. Journal of Materials Science Letters 6(10):1212-1214.

Roman I, Aharonov R (1992) Mechanical interrogation of interfaces in monofilament model composites of continuous SiC fiber-aluminum matrix. Acta Metallurgica Et Materialia 40(3):477-485.

Schadler LS, Giannaris SC, Ajayan PM (1998) Load transfer in carbon nanotube epoxy composites. Applied Physics Letters 73(26):3842-3844.

Schultz J, Lavielle L, Martin C (1987) The role of the interface in carbon fibre-epoxy composites. The Journal of Adhesion 23(1):45.

Shyng Y, Bennett J, Young R, Davies R, Eichhorn S (2006) Analysis of interfacial micromechanics of model composites using synchrotron microfocus X-ray diffraction. Journal of Materials Science 41(20):6813-6821.

Shyng YT, Eichhorn SJ, Young RJ, Davies RJ (2007) Investigation of interfacial stress transfer in a PBO/polypropylene microdroplet composite using synchrotron microfocus X-ray diffraction. Composite Interfaces 14(4):351-359.

Siqueira G, Bras J, Dufresne A (2009) Cellulose whiskers versus microfibrils: Influence of the nature of the nanoparticle and its surface functionalization on the thermal and mechanical properties of nanocomposites. Biomacromolecules 10(2):425-432.

Sirό I, Plackett D (2010) Microfibrillated cellulose and new nanocomposite materials: A review. Cellulose 17(3):459-494.

Stenstad P, Andresen M, Tanem B, Stenius P (2008) Chemical surface modifications of microfibrillated cellulose. Cellulose 15(1):35-45.

Sturcova A, Davies GR, Eichhorn SJ (2005) Elastic modulus and stress-transfer properties of tunicate cellulose whiskers. Biomacromolecules 6(2):1055-1061.

Svagan AJ, Azizi Samir, My A. S., Berglund LA (2007) Biomimetic polysaccharide nanocomposites of high cellulose content and high toughness. Biomacromolecules 8(8):2556-2563.

Tripathi D, Jones FR (1998) Single fibre fragmentation test for assessing adhesion in fibre reinforced composites. Journal of Materials Science 33(1):1-16.

Tullo AH (2002) Breaking the bank with new polymers. Chemical Engineering News 80:13.

Turbak AF, Snyder FW, Sandberg KR (1983) Microfibrillated cellulose, a new cellulose product: Properties, uses, and commercial potential. Journal of Applied Polymer Science: Applied Polymer Symposium 37:815-827.

Tze W, O'Neill S, Tripp C, Gardner D, Shaler S (2007) Evaluation of load transfer in the cellulosic-Fiber/Polymer interphase using a micro-raman tensile test. Wood and Fiber Science 39(1):184-195.

Wagner HD, Lourie O, Feldman Y, Tenne R (1998) Stress-induced fragmentation of multiwall carbon nanotubes in a polymer matrix. Applied Physics Letters 72(2):188-190.

Wagner HD, Vaia RA (2004) Nanocomposites: Issues at the interface. Materials Today 7(11):38-42.

Wang B, Sain M (2007a) The effect of chemically coated nanofiber reinforcement on biopolymer based nanocomposites. BioResources 2(3):371-388.

———. (2007b) Isolation of nanofibers from soybean source and their reinforcing capability on synthetic polymers. Composites Science and Technology 67(11-12):2521-2527.

Wang S, Liang R, Wang B, Zhang C (2008) Load-transfer in functionalized carbon nanotubes/polymer composites. Chemical Physics Letters 457(4-6):371-375.

Wiley JH, Atalla RH (1987) Band assignments in the raman spectra of celluloses. Carbohydrate Research 160:113-129.

Young RJ, Day RJ, Zakikhani M (1990) The structure and deformation behaviour of poly(p-phenylene benzobisoxazole) fibres. Journal of Materials Science 25(1):127-136.

Young RJ, Eichhorn SJ (2007) Deformation mechanisms in polymer fibres and nanocomposites. Polymer 48(1):2-18.

Young RJ, Eichhorn SJ, Shyng Y, Riekel C, Davies RJ (2004) Analysis of stress transfer in two-phase polymer systems using synchrotron microfocus X-ray diffraction. Macromolecules 37(25):9503-9509.

Appendix

Table A. 1 Data for Figure 5.2, which depicts the dependence of the 1095cm^{-1} Raman band shift on the angle of MFC orientation with respect to the tensile axis.

Fiber angle to tensile axis	Raman band shift rate (cm^{-1}/% stain)
2.694	-0.5592
22.865	-0.4783
2.626	-0.7192
25.33	-0.6183
54.7	-0.055
74.48	-0.425
89.044	0.155

Table A. 2 Data for plotting Figure 5.4a, which depicts typical Raman peak shifts of 1095 cm^{-1} with respect to the applied strain on PLA composites of lactide-treated and untreated samples (0.25 wt% loading)

Composite w/ untreated MFC		Composite w/ lactide treated MFC	
Strain (%)	Raman band shift (cm^{-1})	Strain (%)	Raman band shift (cm^{-1})
0	0	0	0
0.25	-0.38	0.25	-0.35
0.25	-0.37	0.25	-0.33
0.5	-0.6	0.5	-0.67
0.5	-0.57	0.5	-0.67
0.75	-0.76	0.75	-0.94
0.75	-0.71	0.75	-0.92
1	-1.01	1	-1.2
1	-0.96	1	-1.15
1.25	-1.2	1.25	-1.34
1.25	-1.16	1.25	-1.3
1.5	-1.25	1.5	-1.46
1.5	-1.21	1.5	-1.29

Table A. 3 Data for plotting Figure 5.4b, which depicts typical Raman peak shifts of 1095 cm^{-1} with respect to the stress on PLA composites of lactide-treated and untreated samples (0.25 wt% loading)

Composite w/ untreated MFC		Composite w/ lactide treated MFC	
Stress(MPa)	Raman band shift (cm^{-1})	Stress(MPa)	Raman band shift (cm^{-1})
0	0	0	0
9.497091	-0.38	6.429261	-0.35
9.081445	-0.37	6.062108	-0.33
20.95247	-0.6	15.0477	-0.67
20.56981	-0.57	14.61221	-0.67
33.43586	-0.76	24.7089	-0.94
32.97984	-0.71	24.21113	-0.92
46.93477	-1.01	34.37609	-1.2
46.35744	-0.96	33.79611	-1.15
59.94815	-1.2	43.5491	-1.34
59.21106	-1.16	42.82769	-1.3
71.18802	-1.25	51.3276	-1.46
70.17128	-1.21	50.34731	-1.29

Table A. 4 Data for plotting Figure 5.5a, which compares Raman band shift of the 1095 cm^{-1} cellulose peak (based on one unit of applied strain) between lactide-treated and untreated MFC fibers (0.25 wt% and 0.5 wt% MFC loading levels) in MFC/PLA composites

Treatment & MFC loading ratio	Average Raman band shift rate (cm^{-1}/% strain)	Raman band shift rate (cm^{-1}/% strain)
Untreated 0.5%MFC	-0.4296	
		-0.3654
		-0.4938
Treated 0.5%MFC	-0.6392	
		-0.5592
		-0.7192
Untreated 0.25%MFC	-0.7501	
		-0.7066
		-0.7818
		-0.7619
Treated 0.25%MFC	-0.86063	
		-0.9068
		-0.8951
		-0.78

Table A. 5 Data for plotting Figure 5.5b, which compares Raman band shift of the 1095 cm^{-1} cellulose peak (based on one unit stress on the composite) between lactide-treated and untreated MFC fibers (0.25 wt% and 0.5 wt% MFC loading levels) in MFC/PLA composites

Treatment & MFC loading ratio	Average Raman band shift rate (cm^{-1}/MPa)	Raman band shift rate (cm^{-1}/MPa)
Untreated 0.5%MFC	-0.01415	-0.0145 -0.0138
Treated 0.5%MFC	-0.0203	-0.0229 -0.0177
Untreated 0.25%MFC	-0.01577	-0.0147 -0.0159 -0.0167
Treated 0.25%MFC	-0.01963	-0.0255 -0.0165 -0.0169

Table A. 6 Data for plotting Figure 5.6 that correlates between apparent modulus and testing temperatures for untreated-MFC/PLA composites (0.25 wt% and 0.5 wt% MFC loading)

Treatment & MFC loading ratio	Temperature (℃)	Modulus at 1% strain (Mpa)
Untreated 0.5%MFC	25.9	3.363
	29	3.168
	27.4	4.539
Untreated 0.25%MFC	28.4	1.421
	26.1	5.811
	22.9	6.755
	25.1	4.992